Report 2005 - 04
June

ILIAS

Ion and Laser beam Interaction and Application Studies

A scientific portrait of the PHELIX theory group

Gesellschaft für Schwerionenforschung mbH
Planckstraße 1 · D-64291 Darmstadt · Germany
Postfach 11 05 52 · D-64220 Darmstadt · Germany

ILIAS

Ion and Laser beam Interaction and Application Studies

I L I A S

Ion and Laser Beam Interaction and Application Studies

The aim of the ILIAS study group

Great machines demand great ideas. Petawatt laser systems have opened new prospectives and extensions into novel parameter regions of many traditional branches of physics:

> Generation of dense and extremely hot plasmas, compact acceleration of electrons and ions, new UV radiation sources, novel atomic physics and collective nuclear processes, among which fast ignition of fusion pellets is of particular relevance.

In 1979 a German Study group was established to investigate the feasibility of inertial confinement fusion with heavy ion beams under the leadership of GSI and funded by the Bundesministerium für Forschung und Technologie, BMFT. Subsequently, this study became the nucleus of a plasma research program *Dense Plasmas Generated by Heavy Ion Beams* and of a Plasma Physics Group at GSI. When considerations for an extension of the GSI accelerator facilities started in the mid nineties, Plasma Physics became one of the main directions of research for this new facility and, a Kilojoule Laser facility was proposed to support the running activities of *warm dense matter*. In following discussions on extending this area of research, a Petawatt High-Energy Laser Facility, PHELIX, was proposed in 1998 which is now under construction and is expected to provide first shots in 2006. Along with the progress of experimental developments a strong obligation was felt to intensify also the theoretical activities in this exciting new field and to focus existing potential and capabilities.

In January 2005 R. Bock (GSI), P. Gibbon (FZ Jülich), J. Maruhn (Univ. Frankfurt), P. Mulser (TU Darmstadt), W. Scheid (Univ. Gießen), and T. Schlegel (GSI) established the ILIAS study group in high power laser interaction theory, with the following goals:

- To disseminate within ILIAS and collaborators the expertise in plasma, atomic, nuclear and nonlinear physics, and numerical simulation techniques held by individual members of the ILIAS study group.

- To coordinate the theoretical activities related to petawatt physics with lasers at GSI.

- To explore the potential of intense laser beams interacting with bulk matter, heavy ion beams and with mass-limited systems and single particles (e.g. cluster, mesoscopic and atomic physics).

- To propose relevant experiments for the PHELIX project and to discuss them in detail with the experimentalists in order to arrive at a coherent, GSI-specific scientific program. In elaborating such a concept the availability of the GSI accelerator system for laser petawatt experiments will play a major role.

- To attract and involve students and young researchers to establish a stable theoretical group of young experts. This goal could be reached within 2 – 3 years from now. To intensify these efforts a regular seminar is already held by the ILIAS members. By individual members pertinent lectures and seminars will be offered at their respective Universities.

In order to to achieve these goals the study group will greatly benefit from the input of ideas by experts at GSI in accelerator, atomic and nuclear physics as well as numerical simulation techniques. Scientific input as well as the enlargement of the ILIAS study group by new members being ready to collaborate, from GSI and from outside, will be highly appreciated.

Organization of the report

1. The ILIAS Theory Group

Present Members

Rudolf Bock
GSI, Planckstr.1, 64291 Darmstadt
Tel.: (0)6159 71 2790, Fax: (0)6159 71 2992
E-mail: r.bock@gsi.de

Paul Gibbon
Complex Atomistic Modelling and Simulation
Central Institute for Applied Mathematics
Research Centre Jülich
52425 Jülich
Tel.: (0)2461 61 1499, Fax: (0)2461 61 6656
E-mail: p.gibbon@fz-juelich.de

Joachim A. Maruhn
Institut für Theoretische Physik
Universität Frankfurt
Max von Laue-Str.1
60438 Frankfurt am Main
Tel.: (0)69 7984 7873, Fax: (0)69 7984 7879
E-mail: maruhn@th.physik.uni-frankfurt.de
Collaborators:
Anna Tauschwitz (née **Kozyreva)**
Tel.: (0)69 7984 7870, Fax: (0) 7984 7879
E-mail: an.tauschwitz@gsi.de

Peter Mulser
Theoretical Quantum Electronics (TQE), Technische Universität Darmstadt,
Schlossgartenstr.7, 64289 Darmstadt
Tel.: (0)6151 16 3079, Fax: (0)6151 16 3079
E-mail: peter.mulser@physik.tu-darmstadt.de

Werner Scheid
Institut für Theoretische Physik
Justus-Liebig-Universität
Heinrich-Buff-Ring 16, 35392 Giessen
Tel.: (0)641 99 33330, Fax: (0)641 99 33339
E-mail: werner.scheid@theo.physik.uni-giessen.de

Theo Schlegel
Theory Division
GSI, Planckstr.1, 64291 Darmstadt
Tel.: (0)6159 71 22796, Fax: (0)6159 71 29012
E-mail: t.schlegel@gsi.de

Scientific expertise (*research profiles of members*)

Rudolf Bock

Consulting

Main organizer of
Plasmaphysik-Seminar at GSI

Paul Gibbon

High-intensity laser interaction with matter
Collisionless absorption in laser-solid interactions
Generation and transport of hot electrons and fast ions
Short pulse hard x-ray generation
Coherent short-wavelength light sources; high-harmonic generation
Laser-based particle acceleration schemes (beat-wave; wakefield)
Nonlinear wave propagation – self-focussing and cavitation
Transport phenomena in strongly coupled plasmas

Numerical techniques
Parallel tree codes; mesh-free plasma simulation
Particle-in-cell simulation
Nonlinear PDEs
Molecular dynamics; Monte-Carlo methods
Lagrangian hydrodynamics
Online visualization and steering

General
Paul Gibbon has worked in the field of high-intensity laser-plasma interactions since the field became experimentally accessible 20 years ago with the invention of chirped pulse amplification. Major contributions include: the first particle-in-cell simulations of **laser absorption** on steep density profiles using a **Lorentz velocity boost** – BOPS [1,2] – a technique which has since become a standard component of high-resolution 1D PIC codes; prediction that **high-order harmonics** well above the nominal cutoff ($\omega p/\omega_0$) can be generated from ionized **solid surfaces** [3]; the first *ab-initio* calculations of **inverse-bremsstrahlung absorption** in **strongly-coupled** plasmas [4]; and semi-analytical modelling of **K-α x-ray and γ-ray bursts** from fs-solid interactions [5,6].

Recent Achievements
More recently this research has focussed on fast algorithmic techniques for handling long-range N-body problems with state-of-the-art supercomputer architectures, in particular hierarchical tree codes. Although commonplace in computational astrophysics, this method represents a completely new paradigm in plasma simulation, offering a powerful mesh-free alternative to the classical Eulerian or Lagrangian meshed-based approaches to modelling Petawatt laser-matter interactions (see [7-11]). Because forces are accurately computed in a tree code, the technique automatically includes collisions, and so can in principle bridge the gap between collisionless PIC and Fokker-Planck simulation. A new magnetoinductive code incorporating this method – PEPC – will be made available to the plasma physics community shortly.

Publications

- on Short Pulse Laser-Matter Interaction:

[1] P. Gibbon and A.R. Bell, *Collisionless absorption in sharp-edged plasmas*, Phys. Rev. Lett. **68**, 1535 (1992).
[2] P. Gibbon, *Efficient production of fast electrons from femtosecond laser interaction with solid targets*, Phys. Rev. Lett. **73**, 664 (1994).
[3] P. Gibbon, *Harmonic generation by femtosecond laser-solid interaction: A coherent 'water-window' light source?* , Phys. Rev. Lett, **76**, 50 (1996).
[4] S. Pfalzner and P. Gibbon, *Direct calculation of inverse bremsstrahlung absorption in strongly-coupled, nonlinearly driven laser-plasmas*, Phys. Rev. E **57**, 4698 (1998).
[5] Ch. Reich, P. Gibbon, I. Uschmann and E. Förster, *Yield optimization and time-structure of femtosecond laser plasma Kα sources*, Phys. Rev. Lett. **84**, 4846 (2000).
[6] H. Schwoerer, P. Gibbon, S. Düsterer, R. Behrens, Ch. Ziener, Ch. Reich, R. Sauerbrey, *MeV x-rays and photoneutrons from femtosecond laser produced plasmas*, Phys. Rev. Lett. **86**, 2321 (2001).

- since 2004:

[7] T. Eickermann, T. Frings, P. Gibbon, L. Kirtchakova, L. Mallmann, A. Visser, *Steering UNICORE Applications with VISIT*, to appear in Phil. Trans. Roc. Soc. (2005).
[8] P. Gibbon, *Resistively enhanced proton acceleration in high intensity laser-foil interactions*, Phys. Rev. E (2004, submitted).
[9] P. Gibbon, F. Beg, E. L. Clark, R. G. Evans, M. Zepf, *Tree-code simulations of proton acceleration from laser-irradiated wire targets*, Phys. Plasmas **11** 4032-4040 (2004).
[10] F. Beg, E. L. Clark, M. S. Wei, A. E. Dangor, R. G. Evans, P. Gibbon, A. Gopal, K. L. Lancaster, P. A. Norreys, M. Tatarakis, M. Zepf, K. Krushelnick, *Return current and proton emission from short pulse laser interactions with wire targets*, Phys. Plasmas **11**, 2806 (2004).
[11] F. N. Beg, M.-S. Wei, A. E. Dangor, A. Gopal, M. Tatarakis, K. Krushelnick, P. Gibbon, E. L. Clark, R. G. Evans, K. L. Lancaster, P. A. Norreys, K. W. Ledingham, P. McKenna and M. Zepf, *Target charging effects on proton acceleration during high intensity short-pulse laser-solid interactions*, Appl. Phys. Lett. **84**, 2766 (2004).

Joachim A. Maruhn
Anna Tauschwitz

The focus of this group's activities have been **hydrodynamic models and simulations**. Since more than 20 years simulations of heavy-ion fusion or experiment-related nature (simulating both actually performed experiments and ones related to future GSI accelerator scenarios) have been done with increasing quality of the codes.
Most of the simulations made use of **codes from Los Alamos** adapted for the specific physics. These were CONCHAS, CAVEAT, and CFDLIB. The latter two codes contain flexible adaptive grids and contain most of the physics needed: various equations of state, viscosity, thermoconductivity, as well as multiple materials. The Frankfurt group principally added the beam-target interaction physics, while the treatment of nonlocal radiation transport is under development.
There is also wide-ranging experience with the **MULTI family of codes** produced by the Madrid group. In the two-dimensional version, the geometry of complex targets can be realized with ease, but a lack of adaptive techniques makes this code less robust with respect

to grid distortions. On the other hand, since radiation transport is already included, this code remains first choice for such problems.
Finally**, view-factor methods** have also been used to study symmetrization in hohlraums. This includes the first coupling of view-factor to hydrodynamic simulations.

Among the **results** obtained by the group are:
- The first simulations showing the **geometry of hydrodynamic flow** in gas targets under heavy-ion irradiation [1].
- Relatively simple calculations showing the **impossibility of direct drive** as envisioned in the HIBALL scenario [2].
- The demonstration of the **necessity of shielding in indirectly driven hohlraum targets** [3].
- The **construction of a hohlraum target** with view-factor methods, including the innovative use of view-factor radiation coupled to hydrodynamically treated walls [4].
- The systematic **effects of beam spatial and temporal structure** on the hydrodynamic flow (e. g., [5]).
- A study of **Rayleigh-Taylor instabilities** using both analytic and numerical methods [6]. For this problem the rezoning properties of the CAVEAT code were absolutely essential.
- A study of the use of **rotating ion beams** to obtain better uniformity in deposition [7].
- The proposal of a **novel target design for equation-of-state measurements** of matter in the WDM regime with the SIS-18 ion beam. Homogeneous target heating is provided by a low-Z tamper, which allows to apply powerful x-ray diagnostics using the PHELIX laser [8].

Publications:

[1] V. Schneider and J. A. Maruhn, *Two-Dimensional Hydrodynamic Simulations of Beam-Target Experiments*, Nuclear Instruments and Methods in Physics Research A **278**, 123 (1989).
[2] G. Buchwald, G. Graebner, J. Theis, J.A. Maruhn, H. Stöcker, and H. Kruse*, Irradiation symmetry of heavy ion driven inertial confinement fusion (ICF) targets*, Laser and Particle Beams **1**, 335 (1983).
[3] K.-J. Lutz, J. A. Maruhn, and R. C. Arnold, *Symmetrization of radiation in heavy ion ICF targets with realistic beam stoppers*, Nuclear Fusion **32**, 1609 (1992).
[4] K. H. Kang and J. A.Maruhn, *Dynamic effects on the symmetrization in indirectly driven ICF hohlraum targets (I),* Fusion Technology **31**, 251 (1997); (II) ibid. 265 (1997).
[5] J. A. Maruhn, K.-J. Lutz, F. Illenberger, and S.Bernard, *Target experiments with intense heavy-ion beams*, Nucl. Inst. Meth. A **415**, 98 (1998).
[6] M. Basko and J. A. Maruhn, *Hydrodynamic instability of shells accelerated by direct ion beam heating*, Phys. Plasmas **9**, 1348 (2002).
[7] M. M. Basko, T. Schlegel, J. Maruhn*, On the symmetry of cylindrical implosions driven by a rotating beam of fast ions*, Phys. Plasmas **11**, 1577 (2004).
[8] A. Kozyreva, M. Basko, F. B. Rosmej, T. Schlegel, A. Tauschwitz, and D. H. H. Hoffmann, *Dynamic confinement of targets heated quasi-isochorically with heavy ion beams,* Phys. Rev. E **68**, 056406 (2003).

Peter Mulser

High-power laser-matter interaction

Ionization dynamics in strong laser fields
Collisional absorption and laser beam propagation
Ablation pressure generation and plasma dynamics
Nonresonant and resonant light pressure effects: laser beam self focusing and parametric instabilities
Collisionless laser beam absorption
Hydrodynamic particle-in-cell code
Dimensional analysis
Nonstandard fluid dynamics
Relativistic plasma physics

Heavy ion beam stopping

Dielectric theory

Peter Mulser has been involved in these kinds of studies since 1966 with laser beams in the intensity range from 10^{10} to 10^{22} W/cm² and pulse lengths from ns to fs. More recent scientific achievements refer to:

Fast ignition studies. As the laser beam cannot penetrate further than up to the relativistic critical density fast ignition with energy deposition in the corona was investigated [1]. It could be shown that the minimum "free" ignition energy and associated "free" intensity are 8 kJ and 2 x 10^{20} W/cm². The minimum density of energy deposition must not be lower than 4 – 5 g/cm³ DT. Owing to unavoidable lateral electron heat dispersion the total deposited energy in the corona required for ignition is not inferior to 50 kJ. Parametric instabilities (stimulated Raman and Brillouin scattering) do not inhibit regular beam propagation in the outer corona. Hole boring is inefficient [2]. The above conditions are such that successful ignition of the compressed pellet core can only be achieved if the stopping of the energetic electrons from the critical region is anomalous. Binary collisions do not effectively stop electrons beyond 1 MeV [2]. The search for anomalous stopping mechanisms is still completely open.

Enhanced collisionless laser beam absorption in clustered media [3, 4, 5, 6]. Nonlinear resonance absorption occurring in the strong laser field represents the main efficient absorption mechanism during the early stage of interaction, typically at times less than 100 fs, when matter has not yet rarefied enough for ordinary linear resonance to take place. During this early stage a single ionized cluster under certain conditions may act as a giant ion charge and increase electron collisionality by orders of magnitude, e.g. factors 10^5.

The physics of collisionless absorption in overdense matter. Irreversibility (heating) in the so-called collisionless laser interaction regime is accomplished by the superposition of the sinusoidal laser field on the collective space charge field of the free electrons [7, 8] Molecular dynamics calculations reveal that among the numerous absorption models proposed ($\boldsymbol{j} \times \boldsymbol{B}$ heating, vacuum heating, surface wave excitation, laser dephasing heating, wave breaking, Brunel effect) the Brunel model is the only one which, after minor corrections, comes close to reality.
A book on *High Power Laser-Matter Interaction* (Springer Verlag) is in preparation.

Publications since 2004:

[1] P. Mulser and D. Bauer, *Fast ignition of fusion pellets with superintense lasers: Concepts, problems and prospectives*, Laser and Particle Beams **22**, 5 (2004).
[2] P. Mulser and R. Schneider, *On the inefficiency of hole boring in fast ignition*, Laser and

Particle Beams 22, 157 (2004).
[3] P. Mulser and M. Kanapathipillai, *Two most efficient nonlinear laser absorption mechanisms in clusters*, submittet to PRL.
[4] M. Kanapathipillai, P. Mulser, and D.H.H. Hoffmann, *Collisionless absorption in clusters out of linear resonance*, accepted by Phys. Rev. A.
[5] M. Kanapathipillai, P. Mulser *et al*., *Net charge of a conducting microsphere embedded in a thermal plasma*, Phys. Plasmas **11**, 3911 (2004).
[6] P. Mulser, *Coherent collisional absorption in clustered media*, Contrib. Plasma Phys. 43, 330 (2003).
[7] D. Bauer and P. Mulser, *Irreversible energy gain by linear and nonlinear oscillations*, accepted by J. Phys.
[8] P. Mulser and D. Bauer, *The collisionless absorption mechanism of superintense laser beams in overdense matter*, submitted to PRL.

Werner Scheid

Besides the main directions of the research group in atomic and nuclear physics, interest is focussed on the **acceleration of electrons by lasers in vacuum** and on the **interaction of intense laser fields with ions**.
The idea of **acceleration of electrons by lasers in vacuum** arose in collaboration with Prof. Hora during the visit of Werner Scheid at the University of New South Wales in Sydney in 1988. We developed programmes for the trajectories of electrons in intense laser fields and for the calculation of stationary electromagnetic beams with finite widths and of light pulses of finite extensions. These programmes were worked out and applied in the diploma and doctoral theses of Thomas Häuser (1993) and Manuel Hölß (1998, 2003) and by the Alexander von Humboldt fellow Dr. Jiaxiang Wang (2000/01). Collaborations on these problems exist with Prof. Hora of the University of New South Wales, with Prof. Ho of the Institute of Modern Physics of the Fudan University in Shanghai and with Dr. Wang of the Center for Nonlinear Studies of the Hong Kong Baptist University. The investigations of the interaction of intense laser fields with ions have their origin in our work on atomic heavy ion reactions. Dr. Carsten Müller and Dr. Alexander Voitkiv (formerly in Giessen, now MPI für Kernphysik in Heidelberg) studied the **creation of electron-positron pairs in collisions of an intense laser beam with a nucleus**. This work is mainly carried out with analytical methods by using
Volkov states. These states are solutions of the Dirac equation describing the interaction of leptons with stationary plane electromagnetic waves. With a three-dimensional numerical lattice method for the solution of the Dirac equation, developed by our group over a longer time period, Manuel Hölß solved the interaction of a laser field with the electron of a hydrogen-like very heavy ion. The corresponding programme can also be used to calculate the higher harmonics of the field created by the interaction.

Publications on:

- Electron acceleration by lasers:

[1] W. Scheid, H. Hora, *On electron acceleration by plane transverse electromagnetic pulses in vacuum*, Laser and Particle Beams **7**, 315 (1989).
[2] Th. Häuser, W. Scheid, H. Hora, *Acceleration of electrons by intense laser pulses in vacuum*, Phys. Lett. A **186, 151** (1994).
[3] J. X. Wang, W. Scheid, M. Hölß, Y. K. Ho, *Mechanism of electron violent acceleration by extra-intense lasers in vacuum*, Phys. Lett. A **280**, 121 (2001).

- Lasers interacting with ions:

[4] C. Müller, A. B. Voitkiv, N. Grün, *Nonlinear bound-free pair creation in the strong electromagnetic fields of a heavy nucleus and an intense X-ray laser*, Phys. Rev. Lett. **91**, 223601 (2003).
[5] M. Hölß, W. Scheid, N. Grün, *Wasserstoffähnliche, schwere Ionen in intensiven Laserfeldern*, Arbeitstagung *Energiereiche atomare Stöße*, Riezlern (2001) EAS 22, page 77.

Theo Schlegel

Opacity calculations
Radiation transport
Radiation hydrodynamics
Short wavelength light sources
High harmonic generation
Long pulse laser-matter interaction

The central topic of interest is the interaction of both intense photon and heavy ion beams with matter. Several scenarios for experiments with an ion beam driver have been developed numerically to reach **matter states of high compression** almost isentropically. Future beam parameters at GSI will allow equation of state studies in unexplored parameter regions.
With the aid of **radiation hydrodynamics** plasma targets with smooth density and temperature profiles will be designed to explore the possibility of heating extended volumes of matter with the kJ PHELIX beam. A hybrid code has been developed to study the symmetrization of radiation in different hohlraum geometries. It solves the 1D hydrodyamic equations, including **advanced multigroup radiation transport** allowing for composite hohlraum walls.

Optimization studies of powerful backscatter have begun in collaboration with the Weizmann Institute in Rehovot/Israel to **diagnose plasma states** produced by intense laser or heavy ion beams. Nonlinear resonant absorption, hot electron production and nonthermal X ray emission has been performed using 1D relativistic PIC codes in combination with a 3D Monte Carlo program. Much attention was also devoted to the study of **production of high harmonics** of the laser radiation from bulk material. Apart from the pure scientific interest this phenomenon represents an interesting light source for a whole variety of applications (ultrafast diagnostics, lithography, attosecond laser pulses). Finally, attention is given to the development of the XFEL laser activities at DESY/Hamburg, as this research field is in many respects complementary to the long wavelength relativistic PHELIX laser interaction.

Intense fs laser pulse interaction with matter is extremely nonlinear. Quantitative understanding is therefore mainly limited to **numerical and simulation approaches**. A firm goal of ILIAS is to develop multidimensional hydrodynamic, particle-in-cell and molecular dynamics modelling capabilities within the next couple of years in order to provide theoretical support for high power PHELIX interaction experiments.

Publications on:

- Matter heating with heavy ions:
See [8] under J. Maruhn and Anna Tauschwitz

- Short pulse laser-solid interaction:
[1] K. Eidmann, J. Meyer-tere-Vehn, T. Schlegel, S. Hüller, *Hydrodynamic simulation of subpicosecond laser interaction with solid-density matter*, Phys. Rev. E **62**, 1202 (2000).

[2] K. Eidmann, R. Rix, T. Schlegel, K. Witte, *Absorption of intense high-contrast sub-picosecond laser pulses in sollid targets*, Europhys. Lett. **55**, 334 (2001).

- K-α production and higher harmonics from short laser pulses:

[3] T. Schlegel, S. Bastiani, L. Gremillet *et al*., *Comparison of measured and calculated X ray and hot electron production in short pulse laser-solid interactions at moderate intensities*, Phys. Rev. E **60**, 2209 (1999).

[4] G. Pretzler, T. Schlegel, E. Fill, D. Eder, *Hot electron gewneration in copper and photopumping of Cobalt*, Phys. Rev. E **62**, 5618 (2000).

[5] U. Teubner, G. Pretzler, T. Schlegel, K. Eidmann. E. Förster, K. Witte*, Anomalies in high-order harmonic generation at relativistic intensities*, Phys. Rev. A **67**, 0133816 (2003).

[6] U. Teubner, K. Eidmann, U. Wagner, U. Andiel, F. Pisani, G. D. Tsakiris, K. Witte, J. Meyer-ter-Vehn, T. Schlegel, E. Förster, *Harmonic emission from the rear side of thin overdense voils irradiated with intense ultrashort laser pulses*, Phys. Rev. Lett. **92**, 185001 (2004).

2. Reporting current progress

P. Gibbon

Mesh-free simulations of laser-proton acceleration with a tree-code

J. A. Maruhn, Anna Tauschwitz *et al.*

Exploration of 3D target simulations
Hydrodynamic instabilities in ion-beam accelerated shells
Two-sided irradiation of cylindrical targets
Isochoric heating of solid targets with laser produced proton beams
Dynamic confinement of targets heated quasi-isochorically with heavy ion beams

P. Mulser

Two most efficient nonlinear laser absorption mechanisms in clusters
Fast ignition: On the inefficiency of hole boring and the problem of energetic electron stopping

W. Scheid *et al.*

Optimum acceleration of electrons with intense lasers in vacuum
Electron-positron creation on highly charged ions with intense laser fields

T. Schlegel *et al.*

Nonlinear resonant absorption, hot electron and Kα production in short-pulse laser-solid interactions at moderate intensities
Simulation of laser-driven X-ray backlighter
Plasma heating with laser-driven hohlraum radiation
Higher harmonics from short-pulse laser irradiation of solid targets

Mesh-free simulations of laser-proton acceleration with a tree code

Paul Gibbon
John von Neumann Institute for Computing, Forschungszentrum Jülich GmbH, D–52425 Jülich

Ion acceleration using short pulse, high intensity lasers focused onto solid targets has received an increasing amount of experimental and theoretical attention over the last five years. This burgeoning interest stems from the huge potential offered by such compact, laser-based MeV proton/ion sources for applications in imaging, hadron therapy, isotope production and nuclear fusion. For all of these applications one needs quantitative knowledge of the ion beam characteristics, such as its energy spectrum, emittance and source size, none of which can be effectively optimized without an understanding of the underlying physics governing the acceleration mechanisms.

To date, this phenomenon has been studied almost exclusively using particle-in-cell (PIC) simulations, which predict that the majority and/or most energetic protons originate from the *rear* of the target surface. This scenario relies on fast (MeV) electrons created via nonlinear heating by the laser on the front of the irradiated target. These pass through the target, setting up a strong, static Debye sheath at the rear, thus pulling ions and proton deposits away from this surface.

Experimental support for this picture has been put forward by the Livermore and Darmstadt groups, citing evidence that: i) protons tend to be emitted normal to the rear surface, even when the latter is at some angle to the front surface; and ii) pre-heating the rear surface—thus cleaning it of hydrocarbon deposits—leads to a strongly reduced proton/ion signal. A sharply contrasting viewpoint has been championed by the Imperial College London, Michigan and lately Osaka groups, who argue that the majority of MeV protons must originate from the *front* (laser-irradiated) side of the target via the collisionless shock driven by the ponderomotive force of the laser.

We have recently examined this issue using a fresh approach; a gridless N-body technique which, although still in a comparatively early stage of development, already overcomes some major limitations of collisionless PIC simulation. Moreover, the control over the plasma collisionality afforded by this method allows us to explore interactions starting from a more realistic, initially 'cold' target state, in which the electrical conductivity of the target is expected to play a major role.

The code used here, PEPC [1], is based on the Barnes-Hut hierarchical tree algorithm [2], implemented in parallel using the hashed oct-tree scheme of Warren & Salmon [3]. Briefly summarized: the electrostatic force-sum on each particle is computed by systematically replacing more distant charges by multipole expansions of charge groups, thus reducing the standard $O(N^2)$ direct sum to an $O(N \log N)$ complexity at the price of a small, controllable error. Discarding the spatial grid allows both electron-ion and electron-electron collisions to be implicitly included in a controlled manner, the details of which will be published elsewhere.

A typical simulation with 3.2×10^6 electrons and ions representing a foil with dimensions $L_x L_y L_z = 5 \times 12 \times 12$ μm^3 at density $n_i = n_e = n_0 = (4 \rightarrow 10)\ n_c$ takes between 60 and 150 (wall-clock) hours on 32 processors of the Jülich IBM p690+ Regatta. Thus, while comprehensive parameter studies with the present code are still beyond reach, preliminary scaling laws can be already be established. Unlike in PIC codes, the electron temperature is not artificially constrained to some value (typically several keV) determined by the mesh size, but can be varied from a few 10s of eV upwards to control the initial target resistivity.

The laser is modeled using a ponderomotive standing wave ansatz for the electromagnetic field E_L applied at the vacuum-plasma boundary on the front-side of the target, a more detailed description of which can also be found elsewhere [5]. For high laser intensities, the profile is typically steepened and driven forwards, so that we also need to track the critical surface when computing the laser fields.

The electrical conductivity of the target, treated here assuming a classical, preionised plasma, determines the magnitude of the return current which can be supplied by the cold background electrons. Previous theoretical and experimental work has demonstrated that resistive effects already inhibit hot electron penetration for intensities as low as 10^{17} Wcm^{-2} . The Spitzer resistivity can be related to the effective collision frequency $\tilde{\nu}_{ei} \equiv \nu_c/\omega_p$ used in the model simply via:

$$\begin{aligned} \eta_e &= \frac{m_e \nu_{ei}}{n_e e^2} = \frac{1}{\omega_p \varepsilon_0} \tilde{\nu}_{ei} \qquad \text{(SI)} \\ &= 6.3 \times 10^{-6} n_{23}^{-1/2} \tilde{\nu}_{ei} \quad \Omega \text{ m}, \qquad (1) \end{aligned}$$

where n_{23} is the electron density in units of 10^{23} cm^{-3}.

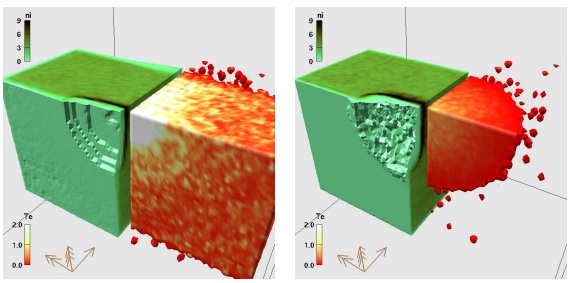

Figure 1: Isovolume sequences of ion density (left; threshold $n_c/20$) and mean electron energy (right; threshold $U_h \geq 10$ keV) sliced half-way through the target in the xz-plane for targets with initial normalized resistivity of a) $\overline{\eta}_e = 7 \times 10^{-3}$ and b) $\overline{\eta}_e = 0.45$. Snapshots are taken at around 90 fs.

To determine how the inhibition of electron transport affects ion acceleration, we compare two simulations with

different target conductivities but otherwise identical parameters: $I\lambda^2 = 2.5 \times 10^{19}$ Wcm$^{-2}\mu$m^2 ($a_0 = 4$), $\sigma_L = 15\ c/\omega_p$, (square) pulse duration $\tau_L = 100$ fs and initial plasma density $n_0/n_c = 4$. The initial electron temperatures in the two cases are 5 keV and 500 eV; the particle diameters $\varepsilon = 3$ and 0.7, giving effective normalized resistivities $\tilde{\eta}_e \equiv \tilde{\nu}_{ei} = 7 \times 10^{-3}$ and 0.45 respectively. For a solid Al target ($n_{23} = 1$), these values would correspond to initial resistivities of 4.4 $\mu\Omega$ cm and 280 $\mu\Omega$ cm respectively.

In the high-temperature case, the effective hot electron range determined by electrostatic stopping is [6] $R_h \approx 80\ \mu$m, so we expect the simulation to behave much like a collisionless PIC code would. This is just what we observe in Fig. 1a), which shows a three-dimensional snapshot of the ion density and hot electron temperature. This plot encapsulates many of the salient features of high-intensity interactions familiar from 2- and 3D PIC simulations to date: bursts of $j \times B$-accelerated electrons generated at 2ω freely traversing the target; formation of a ponderomotively driven ion shock on the front side; and a hot electron Debye sheath being formed on the rear side, pulling ions away from the surface. We also find that the whole foil has been heated to over 50 keV in under 100 fs, in agreement with recent 3D PIC simulations.

Contrast this now with Fig. 1b), a similar sequence for the 500 eV 'resistive' simulation, for which the hot electron range is now $R_h \approx 1.2\ \mu$m . This time we see a completely different picture: despite having energies in the MeV range, the hot electrons are confined to a hemispherical heat-front, 1–2 μm ahead of the shock and are virtually absent from the rear-side vacuum region at this time. This is consistent with Bell's analytical model [6], which predicts a *diffusive* rather than free-streaming transport behaviour at high intensities. The consequences of hot electron transport inhibition for the proton acceleration are self-evident: the absence (or significantly delayed presence) of the hot Debye sheath on the rear side clearly suppresses ion acceleration there. On the other hand, the resistively induced electric field in front of the shock will enhance the front-side acceleration.

These observations are cast in more quantitative form in Fig. 2, which shows how the relative maximum energy of protons originating from the front and rear of the foil respectively *reverses* as the target resistivity is increased.

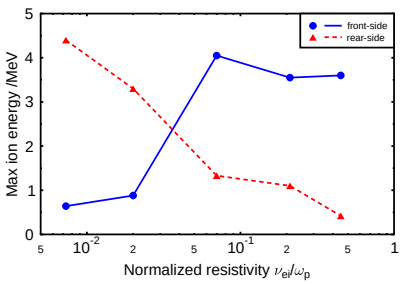

Figure 2: Maximum energy in MeV of protons originating from the front (solid line) and rear (dashed line) of the foil at 150 fs as a function of target resistivity.

Generally, for a fixed set of laser parameters, rear-side sheath acceleration will occur more readily for thin foils, assuming that the contrast ratio is sufficiently high to avoid significant rear-side ablation. For cold, thick targets, only the front-side mechanism will be active: apparently the opposite conclusion of the purely collisionless PIC studies performed to date. This is illustrated by another set of simulations with parameters $d = 10\ \mu$m, $n_e/n_c = 10$, $T_e = 500$ eV, $\omega_p t_L = 450$ (75 fs FWHM), $a_0 = 6, 8$ and a total of 6.72×10^6 particles, ensuring that hot electrons do not reach the rear side of the target in significant numbers, and proton acceleration is confined to the front side, also resulting in a low energy spread or sharp cutoff—Fig. 3.

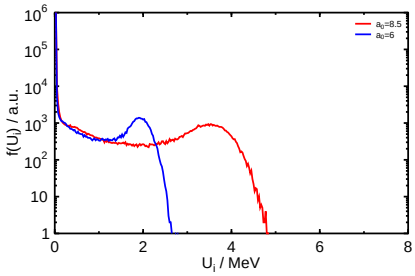

Figure 3: Ion energy spectra showing beam-like emission from front-side protons.

These findings are cleary sensitive to other issues such as the absorption efficiency, hot electron temperature, presence of pre-plasma and the strength of self-induced magnetic fields (which would tend to focus the hot electrons). The interplay between magnetic fields and resistive effects at truly relativistic intensities still remains largely unexplored, however, and a proper assessment of this effect within this model must await the future inclusion of magnetic fields. For the moment, however, the present study suggests that laser-driven proton sources could be optimized by placing a thin hydrocarbon layer (or other proton-loaded coating) onto the front side of an insulating substrate rather than the rear: a conclusion which calls for further experimental investigation.

[1] P. Gibbon, *PEPC: Pretty Efficient Parallel Coulomb-solver*, Tech. Rep. FZJ-ZAM-IB-2003-5, Research Centre Jülich (2003). http://www.fz-juelich.de/zam/docs/printable/ib/ib-03/ib-2003-05.pdf

[2] J. Barnes and P. Hut, Nature **324**, 446 (1986).

[3] M. S. Warren and J. K. Salmon, Comp. Phys. Commun. **87**(266–290) (1995).

[4] S. Pfalzner and P. Gibbon, Comp. Phys. Commun. **79**, 24 (1994).

[5] P. Gibbon, F. N. Beg, R. G. Evans, E. L. Clark, et al., Phys. Plasmas **11**, 4032 (2004).

[6] A. R. Bell, J. R. Davies, S. Guérin, and H. Ruhl, Plasma Phys. Control. Fusion **39**, 653 (1997).

Exploration of 3D Target Simulations

J. A. Maruhn and Th. Schlegel

We investigated the possibility for three-dimensional simulations of ion-beam target interactions using the CFDLIB codes. The principal result is that three-dimensional simulations may well be feasible, but the physics involved should be relatively simple and grid distortion will certainly be a problem.

1. Motivation

Three-dimensional simulations of laser and heavy-ion targets appear to be a natural desideratum, since most experimental situations can be approximated only poorly by calculating two-dimensional cuts. The computational and development efforts for such calculations are, of course, the major obstacle to their broader use. In this work we have made some preliminary exploration into what may be possible with the resources actually available to the community.

2. The *CFDLIB* codes

A newer series of codes continuing the original *Caveat* code [1] as used by the Frankfurt group in many calculations was developped at Los Alamos under the name of *CFDLIB* [2]. These use the same grid techniques, especially the sophisticated ways of rezoning, that characterized *Caveat*, but are in more general in several ways:

- compressible and incompressible flow can be treated,
- a three-dimensional version is available,
- the temperature replaces the total energy as principal variable, making the treatment of heat conduction easier,
- blocks of the computational grid can be distributed in parallel machines,
- multiphase flow can be handled, and
- MHD can be treated (in two dimensions).

3. Code modifications

Since the aim of this work was not to obtain physically relevant simulation results, but to merely get an impression of how much work would be needed to adapt the code and how efficiently it could be run on the computers available locally, we decided to do the minimum modifications necessary to imitate a realistic problem.

The principal work involved implementing the coupling of heavy ion beams to a target. We implemented the beamlet method, but because of the lengthy formulas needed to evaluate the intersection of a line with a a three-dimensional logically cubical zone decided to restrict the beam direction to the *z*-axis direction. Since the faces of a deformed cell are not planar, each face was randomly divided into two triangles. The number of beamlets being much larger than in the two-dimensional case, we also implemented only constant deposition for the time being.

The material was an ideal gas (although the code contains various other analytic equations of state, coupling the SESAME library to it involves some moderate amount of work) with no dissipative processes included.

4. The test calculations

As a simple test case we considered a block of material initially in a block of 40^3 cells and with two heavyion beams impinging from both sides, but displaced to hit the target in neighboring locations. Each beam was simulated by 25 (radial) and 100 (angular) beamlets. All units were taken as arbitrary.

The calculation was done both in an Eulerian and a Lagrangian mode. The Eulerian calculation ran for a long time without encountering any problems, whereas the Lagrangian version ran into grid distortion problems relatively early, which caused difficulties in the deposition routine (final state shown in Fig. 1). If this is not an error in the geometry calculations, it can certainly be remedied by exploiting the rezoning capabilities of the code, although grid distortion will of course be a more serious problem in 3D than 2D.

The calculation could easily be done on a standard (512MB, 2 GHz) PC and took about 25 minutes for 100 time steps. Adding more detailed physics should increase this time by a factor less than 2, so that the future use of 3D simulations will depend mostly on the grid resolution required, since computing time grows in the fourth power of the lnumber of cells in one direction.

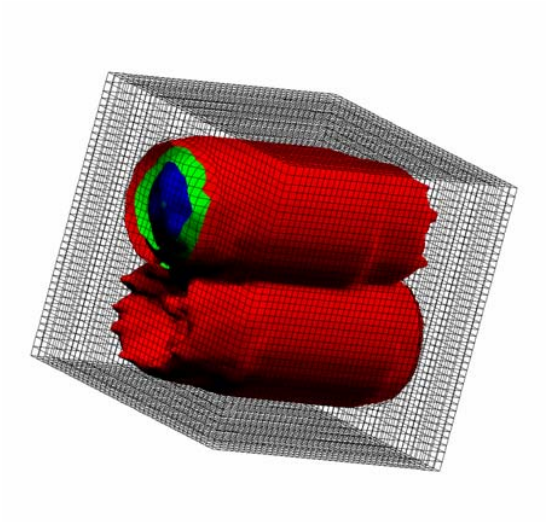

Fig. 1: Contour surfaces of pressure at the end of the Lagrangian test. The grid is plotted as well. The axial asymmetries in the deposition show that the choice of beamlets is not optimal yet.

References

[1] F. L. Addessio et al., Los Alamos Report LA-10613-MS.

[2] J. R. Baumgardner et al., Los Alamos Report LA–UR–90–1361.

Hydrodynamic Instabilities in Ion-Beam Accelerated Shells

M. Basko [1] and J. A. Maruhn

Rayleigh-Taylor instabilities (RTI) are investigated both by analytic techniques and numerical simulations using *Caveat*. A formula derived for the growth rates in initially exponential density profiles turned out to be confirmed quite well by the simulations.

The role of Rayleigh-Taylor instabilities (RTI) in layers accelerated by heating with heavy-ion beams is of obvious importance but has received little attention. Owing to the lack of ablative stabilization, it is of special interest to what extent the density gradient can play a stabilizing role.

We regard the situation shown in Fig. 1: an absorber region is heated by a beam in order to accelerate a payload. Both initial regions may have different densities. Later on, however, part of the heated material leaves the deposition region as pushed-out absorber material. For this general investigation, the ideal gas equation of state was used throughout and the ion beam was coupled into the absorber as a space and time-varying specific power added to the energy balance equation.

An analytic solution was constructed for the unperturbed one-dimensional motion in the case of ideal translational invariance in the x-direction of both the initial configuration and the beam deposition. This was then used as a basis for studying the development of the RTI generated by a small initial perturbation. The analytical solution described a constant acceleration of the payload with spatially homogeneous density in both absorber and payload, linked by exponential increase in the transition region. To produce this idealized solution required a highly specific (but not completely unrealistic) beam profile: a parabolic deposition distribution in space combined with a strong exponential time dependence.

For the case of a continuous exponential density variation, the growth rates were analyzed by Mikaelian [2], although with a fixed width s of the transition layer. Nevertheless, this formula turned out to be even quantitatively useful. For the case of $s \gg h$ the growth rate for the fastest-growing mode is given by

$$\omega^2 = \begin{cases} gk, & 0 < kh < 1/2 \\ \dfrac{g/h}{1+(2kh)^{-2}}, & 1/2 < kh \end{cases} \qquad (1)$$

We performed a series of calculations using a small perturbation in the velocity given by

$$\delta u = 2a_0 k \sin(kx)\exp\left(-k^2(y-h)^2\right) \qquad (2)$$

as the starting configuration. First the accuracy of the numerical method was tested by a series of calculations of the classical RTI with conditions close to a density jump. The classical growth rate was reproduced within about 1% in the linear stage and only in the nonlinear stage did strong deviations occur. Fig. 2 similarly compares some numerical growth rates with the analytical values for the case of homogeneous initial density.

Of even more interest for the applications is the case of a pronounced exponential transition layer. The perturbation continues to grow close to exponentially, but the growth rates show a surprising behavior: they increase by more than 10% between t=2.5 and t=6. This is not due to the expansion of the layer, as shown by the comparison to a situation with a fixed layer thickness (accelerated by a boundary pressure instead of a beam heating). Clearly from among a large number of modes present in the initial perturbation the fastest-growing one emerges relatively late.

The growth rates obtained in the simulations in general are adequately described by the formula (1) scaled down by about 20%. Combining these results for the linear growth rates with a qualitative analysis of the nonlinear regime, we deduce an enhancement of 1.5(h/d) for the distance-moved-over-thickness ratio compared to the discontinuous initial density case (Atwood number 1). With realistic values of h/d=3...5, this is as good as in the best cases of ablative stabilization.

There is the additional problem of beam nonuniformity, which is not directly linked to the RTI (in fact, it can lead to a destruction of the layer even without hydrodynamic instability). Numerical studies for some representative cases showed that 1 to 10% variation in the heating rate may be tolerable.

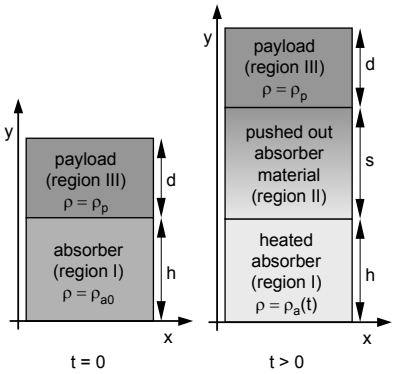

Fig. 1: Layout of the system studied. The lower boundary is assumed to be a motionless plane of symmetry.

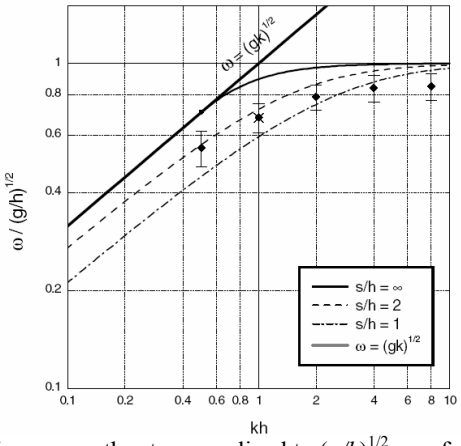

Fig. 2: Linear growth rate normalized to $(g/h)^{1/2}$ as a function of the dimensionless wave number kh. The numerical points are compared to the analytical formulae plotted for three different values of s/h.

References

[1] Permanent address: I.T.E.P., Moscow

[2] K. O. Mikaelian, Phys. Rev. **26**, 2140 (1982).

Two-sided Irradiation of Cylindrical Targets

J. A. Maruhn and H. A. Gutbrod[1]

We study the advantages of two-sided irradiation of targets in a future GSI accelerator scenario. It is found that the homogeneity of the energy deposition as well as the possibility of colliding shocks make this scenario quite attractive.

Unexpected results on the stopping power of nuclei in fully ionized matter [1] invite the idea to study the irradiation of targets by high intensity bunches from opposite directions. This could be done in the proposed accelerator complex at GSI with two heavy ion synchrotrons. Phase-locking the RF of both machines would allow to vary the arrival time on the target and allow to study collisions of shock waves, an important aspect in understanding the dynamics of Supernovae.

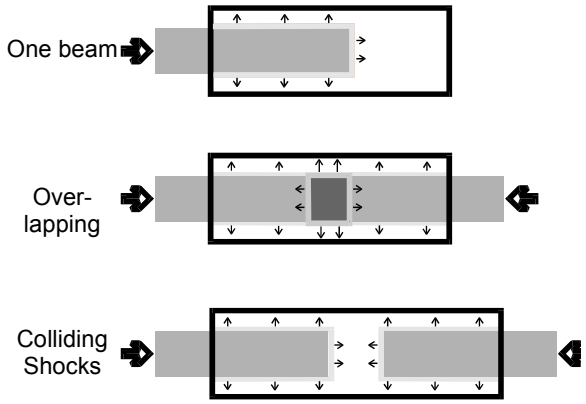

Fig. 1: Irradiation situations tested. The shading illustrates the intensity of the local deposition, and the arrows indicate the shock wave propagation directions.

As a start we have studied the collision of two opposite beams of about equal properties. The first series of simulations were devoted to the possibilities of generating shock waves in quite diverse configurations using two beams. Fig. 1 illustrates the generic possibilities: overlapping the deposition regions yields a localized region of higher temperatures, while separating them leads to the collision of shock waves with possibly higher densities achievable. These cases were compared to that of a one-sided single-beam illumination.

The simulations were carried out using the code *Multi-2D* [2]. The target was a solid gold cylinder of 3 mm radius and with a length adjusted to produce the various situations depicted above (6 mm for the upper two cases, 8 mm for the colliding-beam case). For the beams a flat temporal profile of 19 kJ in 50 ns was assumed and the deposition was calculated based on a SRIM [3] simulation assuming an ion energy of 500 MeV per nucleon, which yields a total range of about 3.5 mm. This ion energy was selected because the range is comparable to the radius, yielding an attractive geometry: for different ion energies effects will be analogous. The total energy corresponds to 10^{12} ions in the pulse.

The radial profile of the beam was taken to be one of two characteristic cases: constant up to the maximum radius of 2 mm or Gaussian with σ=1 mm.

As is well known [4], the two types of radial profile show quite different behavior, but here we concentrate only on the features dues to the new irradiation geometry.

The extreme conditions reached in each case are summarized in the following table:

Beam profile	**Case**	ρ_{max} [g cm^{-3}]	T_{max} [eV]
Flat	single pulse	33.2	10.0
	overlapping	31.6	12.7
	colliding	47.2	10.0
Gaussian	single pulse	33.1	13.8
	overlapping	24.9	17.7
	colliding	40.0	13.8

While the overlapping of the deposition regions seems to offer only the advantage of higher temperatures in the zone of enhanced deposition, the increased density achieved in the colliding shock wave situation is clearly pronounced and it has the additional advantage of being at rest. Fig. 2 illustrates the situation near the moment of highest density for the flat radial profile. The high-density region is a thin sheet at rest in the center of the target but expanding and is at relatively low

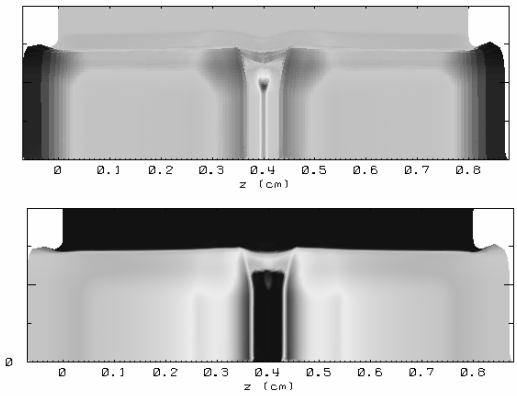

Fig. 2: Grey-scale plot of the density (top) and temperature (bottom) distributions in thew case of colliding shock waves for a flat deposition profile. The geometry is that of Fig. 1. In this grey-scale plot darker areas in the center correspond to higher values, at the border of the target they correspond to low densities in the expansion. The maximum of the density is 47 g/cm^3 and of the temperature 9 eV. The coordinate scale is the same in both directions

temperatures of less than 2 eV.

For the Gaussian beam profile the situation is more complicated and less useful, as illustrated in Fig. 3. Because of the higher speed of the shock waves near the axis of the cylinder, the collision happens first on the axis and then the

[1] GSI

high-density zone expands as a ring to the sides as the collision point moves outward.

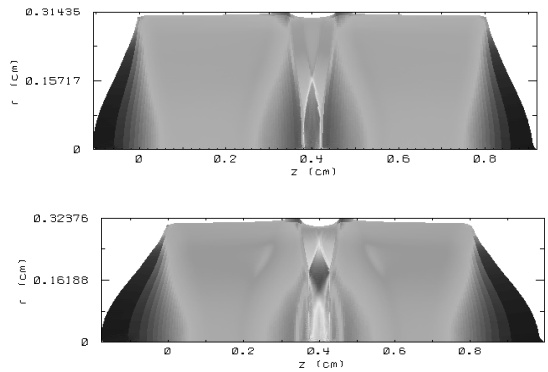

Fig. 3: The development of the high-density region in the Gaussian case. The lower density plot shows a situation about 20 ns later than the upper one.

An additional possible use of overlapping deposition regions could be to heat the target in a more homogeneous way. Although the most prominent feature of the deposition curve is the Bragg peak, it should be noted that the energy loss always has a noticeable slope. To study this effect we compare the energy distribution in a target irradiated from both sides, but only 1.25 mm long in order to avoid the Bragg peaks, with that irradiated by a beam of double the intensity from one side only (see Fig. 4).

While the deposition from both sides does not provide a perfectly homogeneous heating, the advantages are clearly visible: instead of the strongly increasing deposition for a single beam, we get a much more, though not completely,

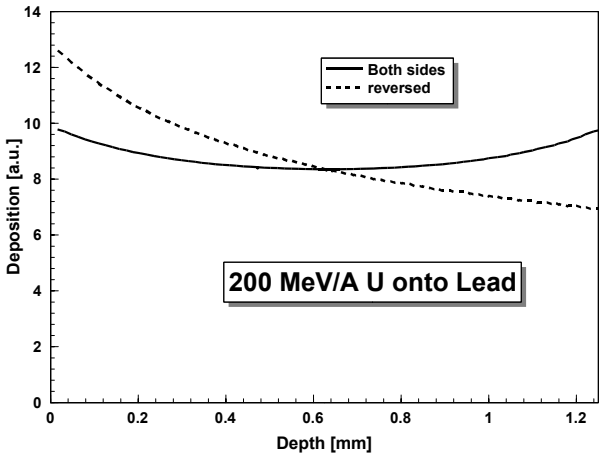

Fig. 4: Deposited energy as a function of the penetration depth of Uranium ions with 200 MeV/A into a solid Lead target with a total length of 1.25 mm. The cases shown are for single-beam irradiation from the left, and for two beams from opposite ends of the target.

constant behavior for the two-sided deposition.. To investigate the practical consequences, we studied a case of a hollow Lead cylinder irradiated by a hollow beam in a configuration very similar to that investigated by Tahir et al. [5]. The simulations were done using Caveat [6].

A hollow Lead cylinder of 0.5 mm inner, 2.5 mm outer radius and 1.25 mm length is irradiated by a beam confined to the

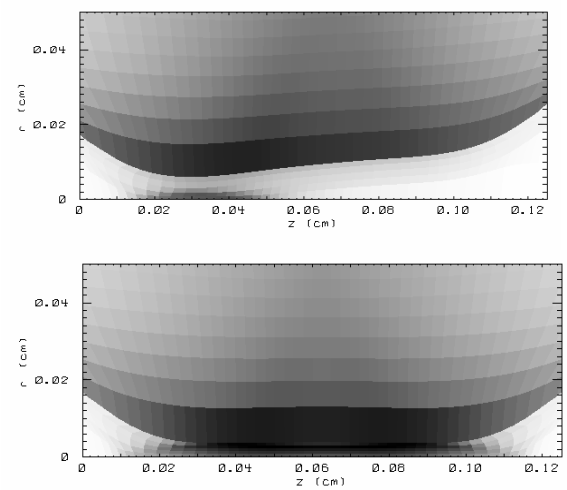

Fig. 5: The inner part of a hollow cylindrical target as discussed in the text approaching convergence on the axis. The colors indicate density with darker colors corresponding to higher densities. The upper plot is for single-sided and the lower one for double-sided illumination by the heavy-ion beams.

radial range 0.5 up to 1.5 mm. The beam consists of Uranium ions with an ion energy of 200 MeV per nucleon delivered over 50 ns. The total beam energy is 1.525 kJ, the temporal deposition profile is parabolic, while the radial one corresponds to an inverted parabola between the inner and outer radii of the beam. The deposition is again computed using SRIM [2].

The hydrodynamic flow caused by the beam converges to the cylinder axis. As expected, the absence of the Bragg peak because of the shorter length of the target makes the inward motion already a bit more uniform. In the case of one-sided illumination, the axis will clearly be hit in a point which moves to the right with time, while for the two-sided illumination there is a much more uniform region of high densities created. Such a gain in uniformity could be essential, e.g., in a scenario of multiply reflected shock waves such as the one proposed by Meyer-ter-Vehn for creating metallic Hydrogen.

Isochoric heating of solid targets with laser produced proton beams

Anna Tauschwitz, E. Brambrink[1], J. A. Maruhn, M. Roth[2], T. Schlegel, Andreas Tauschwitz[3]

A possible target arrangement for equation-of-state measurements with laser accelerated proton beams is discussed. Equation-of-state (EOS) studies of material in the Warm Dense Matter regime is of great importance for astrophysics, geophysics, plasma physics, and inertial confinement fusion research. Isochoric heating of matter by intense particle beams is a fruitful approach for WDM studies because in this case the thermodynamic state of matter is well defined by the target density and the total deposited specific energy. It is however difficult to prepare samples suitable for this kind of measurements due to the stringent requirements on the driver. This problem can be overcome by the use of laser produced proton beams. The proton beam consist of a large number of particles, up to 10^{13}, generated in a short time of < 1 ps and within a spot of 10–50 μm. Unfortunately the protons generated with lasers show a large energy spread with a quasi-exponential spectrum of up to 15-40 MeV, depending on the laser energy. The low energy protons heat the target already in the expansion phase due to the long time of flight.

To chose the experimental conditions for proper EOS measurements, the behavior of proton beam heated matter was studied with the help of the two-dimensional hydrodynamic code MULTI-2D. The code was modified to describe non-monoenergetic beams. The energy change of the proton beam is fast on the hydrodynamic time scale of the heated target. Therefore the proton beam was considered as a group of mono-energetic beamlets within a hydrodynamic timestep. The number of beamlets depends on the cell size in the hydro calculation. The time scale of the heating process depends on the distance between the laser and the proton target.

The PHELIX laser at GSI with 500 J energy, 1 ps pulse length, and focus intensity $I_\mathrm{l} = 10^{20}\,\mathrm{W/cm^2}$ will be available for experiments. In the performed calculations the proton beam parameters for the PHELIX laser are estimated from previous experiments [1]. The proton beam will consist of $5 \cdot 10^{12}$ protons per pulse, having a Boltzmann like energy distribution with a temperature of $T_\mathrm{p} = 18$ MeV and a maximum energy of 40 MeV. The energy dependence of the beam divergence angle and the source spot size were also adopted from experimental data. The beam heats a 20 μm thick aluminum foil which is placed 200 μm away from the primary target emitting the protons. It is assumed that the highest energy protons arrive at the secondary target at $t = 0$. Fig. 1 shows a temperature distribution T along the axis at the rear side of the target at $t = 12$ ps. At this time the protons have an energy $E_\mathrm{p} \simeq 1$ MeV and are stopped in the target. It is seen that for the region near the rear surface of the foil which is no longer heated by the protons, the condition of isochoric heating is satisfied. The temperature distribution is rather homogeneous in a 2 μm thick layer to be used for the EOS

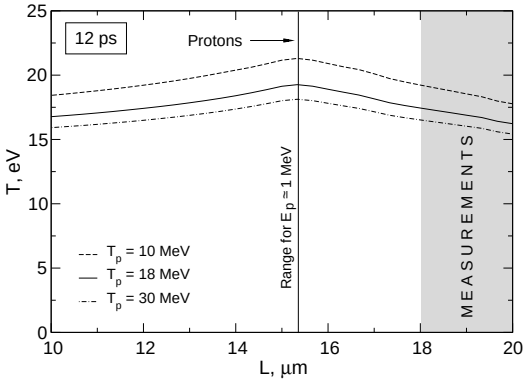

Figure 1: Target temperature along the target axis at $t = 12$ ps. Beam temperature T_p is varied according to different laser intensities.

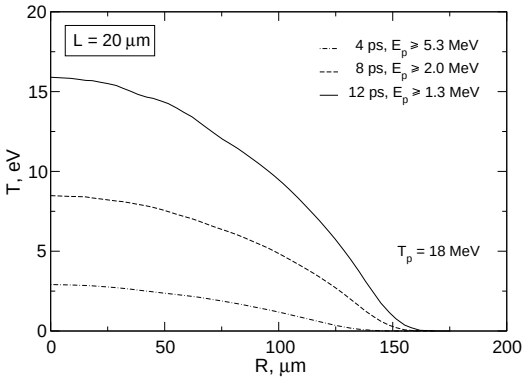

Figure 2: Target temperature vs target radius at $L = 20\,\mu$m for different times.

measurements. Further calculations show that the hydrodynamic expansion at the rear surface of the foil starts around this time. Note that T_p depends on the laser intensity, $T_\mathrm{p} \sim \sqrt{I_\mathrm{l}}$. The target temperature profiles for proton beams with $T_\mathrm{p} = 10$ MeV and 30 MeV show that the laser intensity is not critical for the achievable temperature. Fig. 2 shows the evolution of the radial target temperature distribution at the rear side. It is seen that an isentropic expansion following the isochoric heating will occur for the chosen 2 μm thick layer in a 1D-geometry, so that the measurement of the expansion velocity provides the sound speed in the heated area.

It was demonstrated that the proton beam can be focused using a spherical primary target [2]. Preliminary simulations for this case show much higher temperatures which are strongly dependent on the proton beam focusing.

[1] E. Brambrink, "Untersuchung der Eigenschaften lasererzeugten Ionenstrahlen", PhD thesis, Technical University Darmstadt, 2004.
[2] P. Patel et al., Phys. Rev. Lett **90**, 12 (2003).

[1]LULI, Ecole Polytechnique, France
[2] Technische Universität Darmstadt, Germany
[3]Gesellschaft für Schwerionenforschung Darmstadt, Germany

Dynamic confinement of targets heated quasi-isochorically with heavy ion beams

Anna Tauschwitz, M. Basko[1], F. Rosmej[2], Th. Schlegel, Andreas Tauschwitz[2], D.H.H. Hoffmann[2,3]

A new ion beam target for equation-of-state measurements by X-ray scattering diagnostics is developed. Energetic heavy ions deposit their energy with good uniformity over an extended volume. For energies $E_\mathrm{i} \gtrsim 100\,\mathrm{MeV/u}$ the total deposited specific energy ϵ is known in principle with a good accuracy. When the density ρ_0 of the heated sample remains unchanged, the thermodynamic state of matter after irradiation is completely defined by ϵ and ρ_0. In this case any measured physical quantity is determined as a function of this well defined thermodynamic state.

The governing parameter for volume heating of matter is the specific energy deposition. For our analysis a specific energy of 130 kJ/g deposited in solid hydrogen was chosen. According to the SESEAME equation of state, this corresponds to a temperature of about 0.6 eV (warm dense matter regime), if the beam energy is fully converted into internal energy. A corresponding SIS-18 beam would consist of 8×10^{10} uranium ions of 200 MeV/u focused to a beam spot radius r_b=350 μm (standard deviation of the Gaussian distribution).

The choice of materials for our target is dictated primarily by the proposed method of diagnostics which is based on the measurement of the spectral and angular distributions of x-rays scattered by the heated sample [1]. At GSI, a time-resolved x-ray backlighter (collimated or focused) can be driven by the Phelix laser. However, with probe x-rays in the keV range we are restricted to targets consisting of low-Z elements. It is very advantageous to have a homogeneous density distribution in the target volume for diagnostics and interpretation of the scattering data.

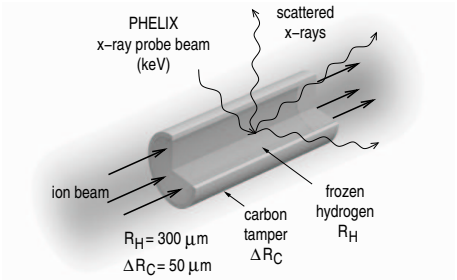

Figure 1: Target configuration for dynamic confinement of frozen hydrogen heated by the ion beam available from the SIS-18, and proposed x-ray diagnostics.

The simplest target for quasi-isochoric experiments would be a bare sample of hydrogen with a radius $R_\mathrm{H} \gtrsim r_\mathrm{b}$ if the density would stay constant in at least a part of the sample. For a rectangular spatial profile of the beam current the density in the center of the heated region remains constant until the rarefaction wave arrives. When the second space derivative of the pressure near the axis is non zero, for a Gaussian profile, the density begins to drop before the rarefaction wave reaches the target center.

[1]Institute for Theoretical and Experimental Physics, Moscow, Russia
[2] Gesellschaft für Schwerionenforschung Darmstadt, Germany
[3] Technische Universität Darmstadt, Germany

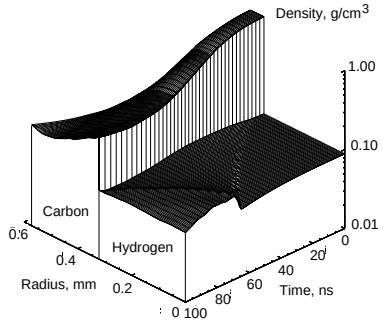

Figure 2: Density distribution vs radius and time for the target shown in Fig. 1, during ion beam irradiation

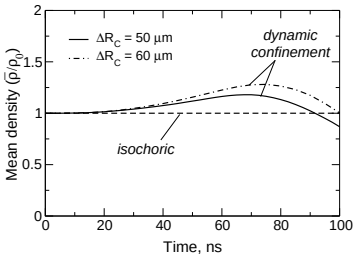

Figure 3: Evolution of the mean hydrogen density during ion beam heating for verying tamper thickness

The adverse effects of the hydrodynamic expansion can be reduced by introducing an appropriate tamper adjacent to the hydrogen. To achieve confinement with a low-Z material transparent for keV x-rays the tamper has to be heated by the wings of the ion beam to produce confining pressure on the main target material (see Fig.1). It is beneficial to use a tamper material with large sublimation energy to delay the beginning of hydrodynamic motion of the tamper. Using the BIG-2 code [2] first simulations have shown that the tamper density should lie below the density of graphite. As an appropriate material carbon phenolic was chosen which has a density of 1.5 g/cm^3 at normal conditions. The overall target behavior is shown in Fig.2. Initially the hydrogen density begins to decrease on the target axis due to the Gaussian heating profile. The pressure in the tamper is higher than in the hydrogen core. The tamper moves inward and launches a weak shock wave. Later on, as the density in the tamper drops, the pressure in the tamper decreases and the motion of the boundary stalls. The reflected shock wave is running outward. At later times the increasing pressure in the core pushes the C/H interface back into its initial position. At the end of the beam our simulation shows the practically uniform density distribution along the radius, as required for diagnostics. In Fig.3 the time evolution of the mean hydrogen density, averaged over the radius is shown. The tamper thickness can be optimized to yield smallest density variation during beam heating ($\Delta R_\mathrm{C} = 50\,\mu$m) or initial denisty at the bunch end ($\Delta R_\mathrm{C} = 60\,\mu$m).

[1] G. Gregori et al., Phys. Rev. E **67**, 026412(2003)
[2] V.E. Fortov et al., Nucl. Sci. Eng. **123** 169(1996)

Two most efficient nonlinear laser absorption mechanisms in clusters

P. Mulser

The author has proposed and studied in detail nonlinear resonance absorption and coherent superposition of electron-ion collisions in ionized clusters to explain the enhanced absorption of ultrashort intense laser beams in clustered matter in the so-called collisionless regime.

Excellent intense laser-matter coupling in clustered media is a well established experimental fact [1]. The physical understanding of the interaction is satisfactory in the multi-photon and field ionization phase. As the kinetic electron temperature T_e approaches 500-1000 eV collisional absorption becomes inefficient. Nevertheless in this so-called collisionless regime light absorption still continues, generally to an extent as to produce most of the heating during this phase, as solidly confirmed by PIC and molecular dynamic (MD) simulations. They show an increase in absorption by orders of magnitude when the molecules of a gas combine to clusters. It is exactly this stage for which analytical modeling is poor and physical understanding is unsatisfactory.

Free electrons can absorb energy from a radiation field either by ballistic interaction with it, i.e. an interaction which is short compared to the laser cycle time $2\pi/\omega$, or by resonant excitation. Since linear resonance occurs at ω_0 which is of the order of the plasma frequency ω_p it can take place after the clusters have sufficiently rarefied, say typically after 100 fs. However, at a sufficiently high laser intensity the single cluster is excited to nonlinear oscillations in the Coulomb type eigenpotential Φ of the charged particles, with the eigenperiod T_0 given by

$$T_0 = \oint dt = \oint \frac{ds}{v} = \oint \frac{ds}{\{\frac{2}{m}(\mathcal{E}-\Phi)\}^{1/2}}.$$

If $\Phi \sim r^2$ (harmonic oscillator) T_0 does not depend on the degree of excitation. If Φ is steeper than r^2, T_0 decreases with the excitation amplitude. However, if Φ is wider than r^2 (the case with Coulomb systems) T_0 decreases and at an appropriate laser intensity enters into resonance with the laser period. This behaviour has extensively been studied in detail. The numerical investigations can be sumarized as follows [2]:

(1) Nonlinear resonance of entire bunches of electrons and of single particles in the collective space charge field is a leading mechanism of collisionless absorption. (2) Almost no irreversible energy gain ("heating") takes place out of resonance. (3) Tidal forces soften and widen the nonresonant-resonant transition. (4) The $\boldsymbol{v} \times \boldsymbol{B}$-force merely leads to a more isotropic electron velocity distribution. (5) The resonant threshold $I_{\rm res}$ is proportional to the square of the cluster radius.

TABLE I: Generalized Coulomb logarithm L_C and amplification factors $g = \nu_{\rm eC}/\nu_{\rm ei}$ for relevant parameters.

			$T_e = 1$ keV			$T_e = 20$ keV		
R nm	Z_C	I Wcm^{-2}	η_C	L_C	**g**	η_C	L_C	**g**
1	210	$\leq 10^{15}$	1.0	2.1	**66**	1.0	3.5	**79**
		10^{17}		3.0	**77**		3.7	**80**
		10^{18}		3.0	**61**		5.2	**103**
5	2.6 $\times 10^4$	$\leq 10^{15}$	0.98	0.1	**4.1×10²**	1.0	1.6	**4.4×10³**
		10^{17}		0.8	**2.3×10³**		1.7	**4.7×10³**
		10^{18}		1.3	**3.2×10³**		3.5	**8.6×10³**
10	2.1 $\times 10^5$	$\leq 10^{15}$	0.43	0.1	**4.9×10²**	1.0	0.6	**1.4×10⁴**
		10^{17}		0.2	**9.5×10²**		0.7	**1.6×10⁴**
		10^{18}		0.3	**1.3×10³**		2.8	**3.4×10⁴**
20	1.7 $\times 10^6$	$\leq 10^{15}$	0.17	0.05	**3.8×10²**	1.0	0.12	**2.2×10⁴**
		10^{17}		0.15	**8.9×10²**		0.12	**2.1×10⁴**
		10^{18}		0.33	**1.6×10³**		1.5	**2.3×10⁵**

The second mechanism whose efficiency we analyze here for the first time is due to the coherent superposition of collisions in clusters. The underlying idea goes back to a proposal for an alternative heating mechanism the author made at a Varenna Intl. Conf. in 1997 in connection with two papers on absorption [3]. The physical principle is again simple. The absorption coefficient α due to collisions in a plasma is proportional to the ion density n_i and the square of the ion charge, $\alpha \sim Z_i^2 n_i$. When N ions cluster together the density of scatterers n_C decreases by N but their charge increases by $Z_i N$ resulting in an increase of $\alpha \sim N$. In order to obtain realistic amplification factors of collisional absorption due to clustering $g = \alpha_C/\alpha$, α_C absorption coefficient of the cluster medium, the fraction ξ of ions combining to clusters, their "outer ionization" degree η_C, i.e. the net charge of the cluster, and the collision frequency $\nu_{\rm eC}$ of an electron with the cluster gas in the presence of the intense laser field need to be known. It holds

$$\nu_e c = \xi \eta_C^2 \frac{Z_C}{Z_i} \frac{L_C}{\ln \Lambda_{\rm ei}} \nu_{ei}, \quad \alpha_{eC} = \frac{\nu_{ec}}{c} \frac{\omega_p^2}{\omega^2}.$$

Λ_{ei} is the Coulomb logarithm of the plasma ions and L_C is the generalized Coulomb logarithm of the clusters, both to be determined selfconsistently. For relevant parameters of cluster sizes R, laser intensities I and electron temperatures T_e the author obtained g factors up to $g = 2.3 \times 10^5$ in a hydrogen gas of 10^{20}cm^{-3} particle density (see Table I)[4].

To illustrate the impact of clustering on absorption the absorption length $L_\alpha = 1/\alpha,\ \alpha = \nu_{ei}\omega_p^2/(c\omega^2)$ for $R = 10$nm, $I = 10^{17}$ W cm^{-2}, $T_e = 20$ keV from Table I is determined. For the hydrogen gas it is $L_\alpha = 4.4$ m. After perfect clustering ($\xi = 1$) it shrinks to $L_{\alpha,C} = L_\alpha/g = 272\mu$m. For $I = 10^{18}$ W cm^{-2} from the last line in Table I $L_\alpha = 13.4$ m shrinks to $L_\alpha/g = 58\mu$m.

In conclusion it has been shown (i) that due to the quadratic dependence of the electron-ion collision frequency $\nu_{\rm ei}$ on the charge number Z of the scatterer there may occur a giant enhancement of this quantity by many orders of magnitude if Z can be increased correspondingly, as for example in clusters, aerosols, sprays, and small droplets of liquids, all of them with $R << \lambda$. (ii) The analysis presented is relevant to light absorption in dusty plasmas. At low laser intensities or high frequencies (X-ray lasers) in Table I the g factors for $I \leq 10^{15}$ Wcm^{-2} ($\hat{v}_{\rm os<v_{th}}$) apply. (iii) Table I gives an indication how, e.g. by using granulated materials, foams, or by seeding, laser-matter coupling with ultra short laser pulses can be improved and thermal electron transport is altered. An estimate of the lifetimes of clusters can be found in [5]. Finally, in collisionless PIC simulations the effect of coherent superposition of collisions is automatically included.

Which of the two effects, nonlinear resonance or coherent superposition of collisions, dominates during the phase of collisionless interaction will depend on parameters like laser intensity, cluster size and laser pulse duration. The first effect may be stronger in large clusters and at earlier times of interaction whereas giant collisional enhancement is favored when the electron cloud has already diffused widely into space, but the ions have not significantly expanded yet.

[1] J.Posthumus (ed.), *Molecules and Clusters in Intense Laser Fields* (Cambridge University Press 2001), Chaps. 5, 6, 7.

[2] M. Kanapathipillai, P. Mulser, and D.H.H. Hoffmann, Phys. Rev. A (accepted for publ.).

[3] T.Ditmire *et al.* in *Super-strong Fields in Plasmas* edited by Lontano, M. *et al.* (AIP conference proceedings 426, American Institute of Physics, New York, 1998) p.354.

[4] M.H.R.Hutchinson *et al.* in *Super-strong Fields in Plasmas* edited by Lontano *et al.* (AIP conference proceedings 426, American Institute of Physics, New York, 1998) p.314.

[5] P. Mulser and M. Kanapatipillai, Phys. Rev. Lett. (accepted for publ.).

[6] M.Kanapathipillai, P.Mulser *et al. Phys. Plasmas* **11**, 3911 (2004).

Fast ignition: On the inefficiency of hole boring and the problem of energetic electron stopping

P. Mulser

On the basis of present knowledge on electron beam-plasma coupling it follows that in fast ignition with energies not exceeding 100 kJ hole boring and fast ignition exclude each other. Successful ignition of the precompressed pellet core requires anomalous, i.e. collective, electron beam-pellet interaction.

The concept of fast ignition (FI) is attractive because it offers several advantages: (1) high burn efficiency (25%), (2) no special symmetry constraints, and (3) reduced growth of hydrodynamic instabilities. However, the advantages contrast with the fact that the laser can deposit its energy at densities not exceeding the critical density ρ_c, respectively particle density n_c. As a consequence, electrons of relativistic energies must provide for the energy transport to the dense compressed fuel in an efficient way, that is, good collimation, and on a time scale of several tens of ps (e.g. 70 ps) [1,2]. In this scheme of fast coronal ignition (FCI; Fig. 1) it would be most advantageous to bring the laser energy deposition region as close as possible to the high density core of $\rho = 200\,\mathrm{g/cm^3}$ DT fuel by hole boring. Its efficiency can be studied analytically by the fluid model of bow shock generation by the laser radiation pressure p_L (Fig. 2(a)) or by studying the penetration of a solid cone of half aperture angle ϑ driven by p_L (Fig. 2(b), (c), (d)) [3]. Hole boring is most efficient in cold matter with negligible counter pressure p_0. To the author's surprise however even in this case hole boring at the spectacular beam intensity of $I = 10^{21}\mathrm{W/cm^2}$ stops latest at $\rho = 80\,\mathrm{g/cm^3} \ll 200\,\mathrm{g/cm^3}$ in both models [3]. In all realistic situations the bow shock or solid cone runs into preheated matter. With the help of flux limited Spitzer type electronic heat conduction p_0 reaches such values that with $I = 10^{21}\mathrm{W/cm^2}$ hole boring stops at the vanishing depth of about $5\,\mu$m [3] corresponding to a few grams/cc DT. This is in perfect agreement with what was observed in our numerical simulations under all circumstances [1]. In conclusion, the energy requirements are such that the average kinetic energy of the electrons created by Nd, Ti:Sa or iodine lasers is too high to allow stopping in the precompressed pellet by binary collisions. In this situation of weak electron-pellet interaction, moderate hole boring, induced mainly by light pressure, takes place but pellet ignition fails. At laser beam wavelengths $\lambda \sim \lambda_{\mathrm{Nd}/4}$ (KrF) pellet ignition cannot be categorically excluded on the basis of collisional interaction only. However, then very quickly a thermal pressure exceeding the light pressure is generated and hole boring is stopped. Numerical studies confirm the analytical findings.

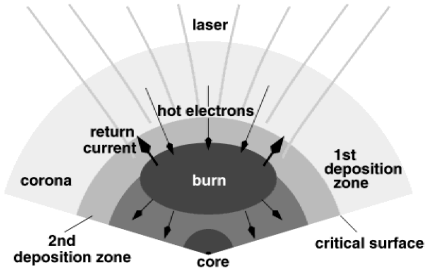

FIG. 1: Fast coronal ignition (FCI) scheme. Hot electrons provide for the necessary energy transport from the first to the second energy deposition zone.

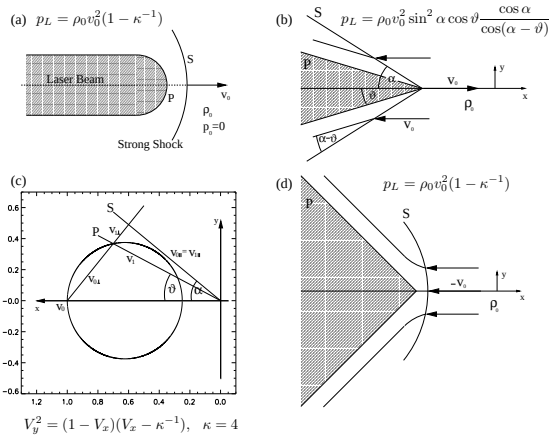

FIG. 2: Holeboring in cold matter: alternative models for matter displacement. (a) laser acts as impermeable piston; P piston pressure, ρ_0 undisturbed precompressed pellet density, v_0 hole boring speed. Oblique shock (b) is determined from the shock polar (c). Beyond limiting angle ϑ shock detaches from cone (d).

[1] S. Hain and P. Mulser, Phys. Rev. Lett. **86**, 1015 (2000).
[2] P. Mulser and D. Bauer, Laser and Particle Beams **22**, 5 (2004).
[3] P. Mulser and R. Schneider, Laser and Particle Beams **22**, 157 (2004).

Optimum acceleration of electrons with intense lasers in vacuum

Werner Scheid

The acceleration of electrons in the vaccum by electromagnetic waves inside a half wavelength is discussed. TeV electrons can be obtained by short intense laser pulses.

Acceleration of electrons by laser light plays a major role in the development of future accelerators with extremely high energies. We studied the acceleration of electrons in the longitudinal direction by a linearly polarized transverse electromagnetic field [1, 2] and by finite laser pulses [3] in vacuum.

Assuming the z-direction as the direction of progression of the transverse wave and the x-direction as the direction of the electric field, we can write the electric and magnetic fields as follows:

$$\boldsymbol{E} = E_x(z-ct)\boldsymbol{e}_x, \quad \boldsymbol{H} = H_y(z-ct)\boldsymbol{e}_y, \tag{1}$$

with $E_x(z-ct) = H_y(z-ct)$. The equation of motion for the electron with rest mass m is

$$\frac{d(m\gamma\boldsymbol{v})}{dt} = -e\left(\boldsymbol{E} + \frac{\boldsymbol{v}}{c}\times\boldsymbol{H}\right) \tag{2}$$

The integration of the equation of motion yields the Lorentz factor γ for the electron under the initial conditions $\boldsymbol{r}(t=0) = 0$ and $\boldsymbol{v}(t=0) = 0$:

$$\gamma = 1 + \frac{1}{2}A^2(u) \tag{3}$$

$$\text{with} \quad A(u) = \frac{e}{mc^2}\int_0^u E_x(u')du', \quad u = z - ct.$$

As an example let us consider a laser field of a length of a half wavelength crossing the electron:

$$\begin{aligned} E_x &= -E_0 sin(kz-\omega t) \\ &\quad \times (\Theta(z-ct+\lambda/2) - \Theta(z-ct)). \end{aligned} \tag{4}$$

With eq. (3) we find a Lorentz factor

$$\gamma = 1 + \frac{1}{2}(\delta\lambda/\pi)^2, \tag{5}$$

where $\delta = eE_0/(mc^2)$ is the ratio of work of the field E_0 per length unit crossing the electron to the rest energy of the electron. After the laser wave (4) has crossed the electron, the electron has moved the distances ($y = 0$)

$$z = \frac{3}{16}(\gamma-1)\lambda \tag{6}$$

$$x = -\frac{1}{\sqrt{8}}(\gamma-1)^{1/2}\lambda. \tag{7}$$

Therefore, the length of an accelerator would be $L = \frac{3}{16}(\gamma-1)\lambda$ with an energy gain of kinetic energy $T/L \approx \frac{16}{3}mc^2/\lambda$.

Let us consider numerical examples. If we set the intensity (SI-units)

$$\begin{aligned} I &= 0.5c\varepsilon_0 E_0^2 \\ &= (\frac{\varepsilon_0}{\mu_0})^{1/2}(\frac{mc^2}{e})^2\pi^2\frac{\gamma-1}{\lambda^2} = 6.84\times10^9\mathrm{W}(\gamma-1)/\lambda^2, \end{aligned} \tag{8}$$

take a neodymium glass laser with $\lambda = 1.06$ μm and assume $\gamma = 10^6$, corresponding to 0.511 TeV electrons, the acceleration length is $L = 0.199$ m, the energy gain $T/L = 2.57$ TeV/m and the laser intensity $I = 6.09\times10^{23}$ W/cm^2. For an intensity of $I = 10^{22}$ W/cm^2, we find $\gamma = 1.6\times10^4$ and $L = 3.3$ mm.

Since the electron moves slightly in transversal direction, one may think on a cylindrical laser beam with such a finite radius R that the electron can leave the beam after a half wavelength of the laser field has accelerated it. By use of eq. (7) this radius is obtained as $R \approx \delta\lambda^2/(4\pi)$. Then the corresponding laser power is $P = \pi R^2 I$, and the Lorentz factor can be written as

$$\gamma = 1 + \frac{4\sqrt{2}e}{mc^{5/2}\pi}\sqrt{P} = 1 + \sqrt{\frac{P}{2.7\times10^9\ \mathrm{W}}}. \tag{9}$$

This expression for γ is independent of the wavelength of the laser beam and yields TeV electrons for $P \approx 10^{22}$ W.

A problem is to inject the electrons into the intense laser field. To study this problem we first considered the fields of a beam with finite width. For that we solved the Maxwellian equations in the paraxial approximation and by the angular spectrum method which is an exact solution, but finally leading to numerical integrations. The idea is to let the electron incident into the laser beam from the sideways direction which is called the "capture and acceleration scenario" (CAS) by Y. K. Ho [4]. In most cases this processes leads to a reflection of the electron by the laser beam. Under certain incident angles the electron is captured and a very moderate acceleration occurs in the surface part of the laser beam.

A promising proposal is to apply a short laser pulse running over an electron. The pulse has to be formed with a steep rise of the field strength inside a half wavelength with additional minor oscillations which would not disturb anymore the motion of the electron. Calculations for such an arrangement were done for $Q = \delta\lambda/(2\pi) = 10$ in [3] and an acceleration of $\gamma \approx 30$ was obtained in comparison with $\gamma = 201$ according to eq. (5). Intense laser pulses consisting of one or two wavelengths running over electrons seem to be the best possibility to accelerate electron bundles to TeV energies.

[1] W. Scheid and H. Hora, Laser and Particle Beams **7** (1989) 315-332

[2] Th. Häuser, W. Scheid and H.Hora, Phys. Lett. A **186** (1994) 189-192

[3] J. X. Wang, W. Scheid, M. Hoelss and Y. K. Ho, Phys. Lett. A **275** (2000) 323-328

[4] P. X. Wang, Y. K. Ho *at al.*, J. Applied Phys. **91** (2002) 856-866

Electron-positron creation on highly charged ions with intense laser fields*

Carsten Müller[1,2], Alexander Voitkiv[1], and Norbert Grün[2]

[1]Max-Planck-Institut für Kernphysik, Saupfercheckweg 1, 69117 Heidelberg; [2]Institut für Theoretische Physik, Justus-Liebig-Universität Giessen, Heinrich-Buff-Ring 16, 35392 Giessen

Electron-positron pair production is studied in the collision of a nucleus with a laser pulse.

Electron-positron pairs can be created in the collision of a relativistic heavy nucleus with an intense laser field. Within the Dirac sea picture, the process of pair production can be explained as the transition of an electron from the negative-energy continuum into a positive-energy continuum state or a bound state around the nucleus with charge Ze. This process is induced by the absorption of n photons of the laser with a frequency ω_L' in the rest system of the nucleus:

$$Z + n\omega_L' \to Z + e^+e^-. \tag{1}$$

If the nucleus runs towards the laser beam, the photons undergo a Doppler shift with the frequency ω_L' related to the frequency ω_L of the laser light in the coordinate system were the nucleus is moving with a velocity v: $\omega_L' = (1+\beta)\gamma\omega_L$ with $\beta = v/c$ and $\gamma = (1-\beta^2)^{-1/2}$.

In order to treat the pair creation we consider the interaction of the leptons with the combined electromagnetic fields of the nucleus and laser wave in the rest system of the nucleus [1, 2]. The transition amplitude between the initial and final state can be formulated in the prior form as

$$(S-1)_{fi} = -\frac{ie}{\hbar c}\int \Psi_f^\dagger (Z/|x|)\psi_{p,s}^{(+)} d^4x. \tag{2}$$

Here, $\psi_{p,s}^{(+)}$ represents a negative-continuum Volkov state describing the outgoing positron in the field of a plane laser wave, but not in the field of the nucleus producing the transition. The wave function Ψ_f represents the eigensolution of the total Hamiltonian and describes the produced electron. We employ physically reasonable approximations for Ψ_f, namely $\Psi_f = \psi_{p,s}^{(-)}$ corresponding to a positive-continuum Volkov state for the case of free-free pair production and $\Psi_f = \phi_{1s}$ for bound-free pair production when the electron is bound in the 1s state of the hydrogen-like ion.

This theory was applied [1, 2] to the collision of a nucleus of charge number $Z = 50$, moving at a Lorentz factor of $\gamma = 50$, with an intense, circularly polarized XFEL (x-ray free-electron laser) beam of photon energy $\hbar\omega_L = 9$ keV and intensity parameter $\xi = eF/(m\omega_L c) = 7.5\times10^{-4}$, which corresponds to an electric field strength of $F = 1.75\times10^{13}$ V/m and an intensity of nearly 10^{24} W/m^2. In the nuclear rest frame, the photon energy as well as the laser field strength are enhanced by a factor of 100 and amount to $\hbar\omega_L' = 900$ keV and $F' = 1.75\times10^{15}$ V/m. In comparison, the Coulomb field of the $Z = 50$ nucleus at the K shell radius $r_K \approx 10^{-12}$ m is about a factor of 40 larger than the strength of the laser field. In order to surmount the energetic threshold for pair creation, the absorption of only two photons is necessary.

*Communicated by Werner Scheid

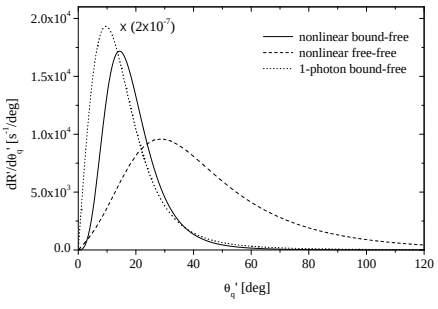

Figure 1: Angular differential rates in the nucleus frame for two-photon (or nonlinear) bound-free and free-free pair production. Also shown is the rate for bound-free pair creation by the absorption of a single photon of 18 keV.

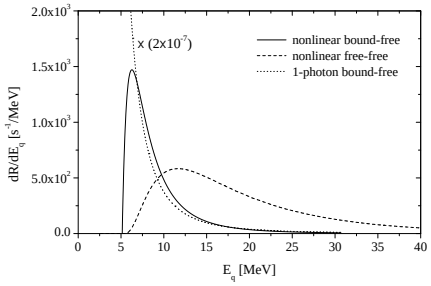

Figure 2: Energy differential rates for pair creation in the laboratory system

Fig. 1 shows the angular distribution of the positrons in the nuclear rest frame. The angle θ_q' is measured with respect to the laser propagation direction. The different spectra are calculated for bound-free and free-free pair production by absorption of two photons and for bound-free pair creation by absorption of one photon with an energy of 18 keV. Fig. 2 shows the energy distributions of the positrons in the laboratory system for these cases. The energies of the positrons from the bound-free pair creation are about 6 MeV $\le E_q \le$ 12 MeV, which is smaller than the energies of the positrons from free-free pair production which amount 7 MeV $\le E_q \le$ 30 MeV. If the spectra are integrated, we find a total rate of 6.5×10^3 s^{-1} for bound-free pair production and of 9.6×10^3 s^{-1} for free-free pair production in the laboratory system. This means that a laser pulse (9 keV) of 100 fs generates about 10^{-9} pairs by two-photon absorption. The rate of the one-photon absorption (18 keV) is about 10^{10} s^{-1}.

[1] C. Müller, A. B. Voitkiv, and N. Grün, Phys. Rev. Lett. **91** (2003) 223601

[2] C. Müller, A. B. Voitkiv, and N. Grün, Phys. Rev. A **70** (2004) 023412

Nonlinear resonant absorption, hot electron and K α production in short-pulse laser-solid interactions at moderate intensities

T. Schlegel, S. Bastiani, L. Gremillet, J.-C. Gauthier

When an intense laser pulse is focused onto a solid target, a plasma is produced which is heated up to hundreds of eVs, depending on the absorbed laser intensity. Thermal x-rays at energies above 1 keV are produced. To get a higher x-ray radiation yield, target illumination with p-polarized laser light has to be used. Then, collisionless absorption processes become dominant in the laser energy deposition, and in their nonlinear regime, produce hot electrons, which give rise to bremsstrahlung and K α radiation from the target bulk. This nonthermal emission has a relatively short duration, comparable to that of the incident laser pulse. The plasma properties strongly depend on the temporal shape and the contrast ratio of the intense laser pulse. A controlled prepulse can generate preformed plasmas with distinct density scale lengths. Experiments have shown that fast electron production and nonthermal K α emission peak for a plasma scale length, where resonant absorption is maximized [1].

To investigate the scale-length dependence of observables such as the laser absorption, energy distribution of electrons and ions inside the plasma and on the rear side of the target (overdense plasma), and mean energy and directionality of the electrons, particle-in-cell (PIC) simulations with the 1D relativistic code EUTERPE [2] were performed. A p-polarized laser pulse with $\sin^2$ temporal shape, a duration of 120 fs (FWHM) and a peak intensity 4×10^{16} W/cm^2 strikes a solid target with maximum plasma density (27) n_c and an exponential density profile under 45^o. Electron and ion temperatures of 500 eV respectively 100 eV are supposed, following hydrosimulations of the prepulse-target interaction with parameters of the experiment [1]. Electrons, reaching the rear surface of the bulk target, are reinjected with their initial momentum distribution, the ions are mobile.

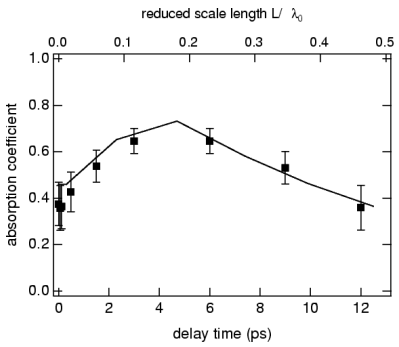

Figure 1: Laser light absorption of the main pulse as a function of time after the prepulse (or the reduced scale length). The squares show the experimental values.

Fig. 1 gives the absorption coefficient in dependence on delay time or density scale length $L = n_c/|dn/dx|_c$ normalized to the vacuum laser wavelength λ_0. The experimentally observed maximum at $L/\lambda_0 \approx 0.2$ with a value between 0.6 and 0.7 is confirmed. Because the PIC code self-consistently solves the Poisson equation, one can study the ambipolar fields generated in the collective interaction processes including their nonlinear regime, where the strong electrostatic plasma wave breaks. Different physical situations obtained while varying the initial scale length are collected in Fig. 2. For three values of L/λ_0 0.01, 0.2 and 0.6 the longitudinal electric field E_x (solid lines), directed normally to the target surface, is shown at the time where the the resonance field is close to its maximum. We see a large resonance for L/λ_0 0.2 after the field has tunneled from the turning point to the critical surface. Since the distance between these two points increased in the case of L/λ_0 0.6, the resonance becomes weaker, as expected. In the overcritical plasma, strong electrostatic field perturbations with the local plasma frequency can be observed. These disturbances are caused by the jets of energetic electrons flowing in the bulk of the target. From the existence of similar perturbations in the transverse field pattern inside the target, we can conclude that a strong directionality of the fast electron jets occurs.

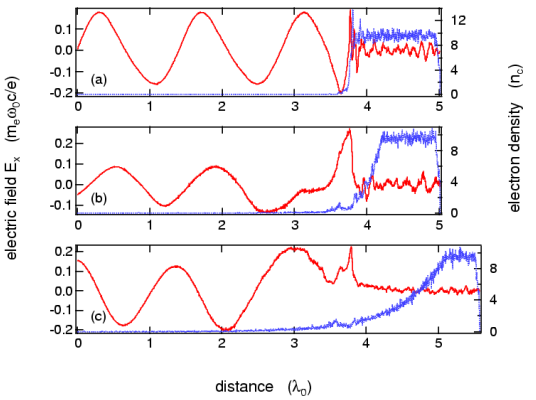

Figure 2: Longitudinal electric field (solid line) and electron density profiles (dotted line) for three different initial gradient scale lengths: (a) L/λ_0 0.01, (b) L/λ_0 0.2, and (c) L/λ_0 0.6.

In addition to the field distribution, the electron density profile is also shown in Fig. 2. When the scale length is increased, an undercritical plasma shelf develops, expands, and eventuelly becomes overcritical somewhere in front of the critical surface. At the same time, the plasma profile is steepened on the dense plasma side. This results from the well-known action of the ponderomotive force of the resonant field.

The number of electrons reaching the right boundary of the simulation box (rear target surface) is plotted in Fig. 3, per keV and per cm^2 of target surface as a function of energy, for several scale lengths. We distinguish three different energy ranges. At very low energy, less than 1 keV, we have thermal electrons characterized by their initial tem-

perature $T_e \approx 600$eV. Then there appears a local plateau of electrons with energies $E \approx (5$–$10)$ eV and a high energy tail of the distribution function follows. This tail is rather noisy but this cannot be avoided in PIC simulations because of the relatively small number of particles. Additional fluctuations can be produced by interaction of the fast electrons with the electron-excited plasma oscillations in the overdense target. To understand how electrons can

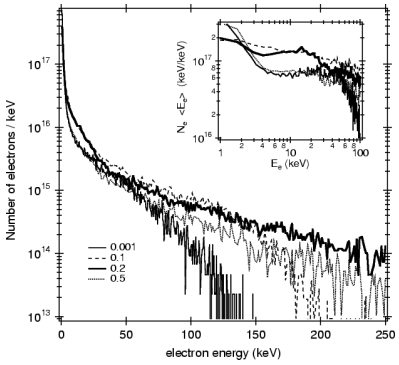

Figure 3: Number of electrons flowing through the right (overdense) edge of the simulation box, per keV and per cm^2 of the target surface, as a function of kinetic energy for several values of the initial scale length. The inset shows the distribution of the electron energies as a function of electron energy.

gain energy of some hundred keV at laser intensities in the $\approx 10^{16}$ W/cm^2 range (i.e., quiver electron energies of a few keV), we follow some "test" electrons in their interaction with the laser and the laser-driven plasma wave. In Fig. 4, the trajectory of one such electron is plotted in the electric field E_x. The motion of the particles in the resonance region is strongly dependent on their "phase matching" with the plasma wave. The figure contains, besides the electric field, time-history plots of the kinetic energy of the test particle, together with the electron density it "sees" during its motion.

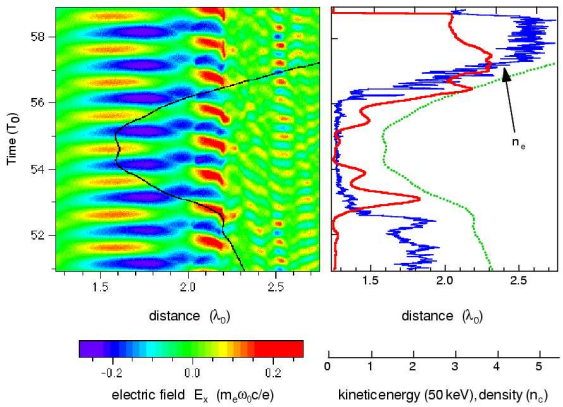

Figure 4: Trajectory of a test electron as a function of space in wavelength units and as a funtion of time in laser periods. The longitudinal electric field is superimposed. On the right, the electron density (blue line) and the kinetic energy (red line) of this test particle are shown with its trajectory. Reduced initial scale length $L/\lambda_0 \approx 0.2$.

The labeled electron starts with thermal energy at the entrance of the resonant field, becomes trapped in the plasma wave and is accelerated to an energy of the order of ≈ 100 eV. The electron makes a large excursion in front of the target during the next two laser cycles. This behaviour can be described as the formation of "cloud" electrons which do not return to the target bulk during the same laser cycle where they originated. On its way back to the target, the test electron arrives to the critical surface just in phase with the negative half-period of the resonance field, and gets an additional "kick" of more than ≈ 50 eV. Slightly decelerated by the resonance of the next cycle, its velocity is increased again in the plasma wave field (seen as undulations in the target bulk in Fig. 4) up to ≈ 200 eV. Continuing its motion in the bulk of the target, part of this energy is converted into electrostatic energy of the dense plasma oscillations. Only a relatively small number of electrons will have the right "phase" with respect to the resonant field to be accelerated to such large energies. A very much larger number of electrons will be resonantly heated to energies in the range between 10 and ≈ 40 eV (see Fig. 3).

Using a 3D Monte Carlo code [3] in a relativistic extension as well as stopping power and opacity data corresponding to the SiO_2 targets shot in the experiments, we also can obtain results on K α emission following the removal of a K-shell electron. The code takes into account the opacity of the material located between the point of emission and the point of observation, at any angle with respect to the target normal. The knowledge of K α output for a chosen material given in numbers of photons per electron delivered in one steradian allows us to calculate the absolute number of produced K α x-ray photons. To get the integral photon number per steradian we have to convolve the K α yield with the electron distributions shown in Fig. 3. The calculated K α photon numbers for several values of the delay time after the prepulse together with calibrated measurements are given in Fig. 5. These results are normalized to 1 J of incident laser energy.

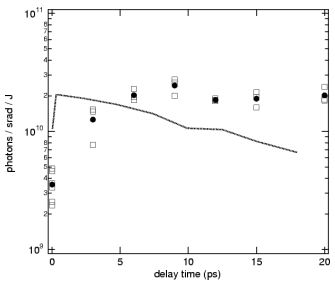

Figure 5: Simulated K α photon yield (dotted line) as a function of the delay time together with experimental values in SiO_2.

A qualitative agreement with the calibrated experimental values was achieved for prepulse delays exceeding 4–5 ps. The maximum number of measured photons of $\approx 10^{10}$photons/sr/J could be reproduced without any adjustable parameter used.

[1] S. Bastiani et al., Phys. Rev. E, **56**, 7179 (1997).
[2] G. Bonnaud, G. Reisse, Nucl. Fusion, **26**, 633 (1986).
[3] A. Rousse et al., Phys. Rev. E, **50**, 2200 (1994).

Simulation of laser-driven x-ray backlighter

V. I. Fisher [1], D. V. Fisher [1, 2], Y. Maron [1], T. Schlegel and D. H. H. Hoffmann

One of applications proposed for PHELIX is ignition of hot laser sparks for x-ray shadowgraphy and K-shell absorption spectroscopy of heavy-ion-beam targets [1]. In 2004 we started numerical simulation and optimization of laser-driven x-ray backlighter. An emphasis of this study is on efficiency of conversion of the laser pulse energy into hard x-rays. Here we present the computational tools and first results.

The simulation is performed in two steps. First, the laser-foil interaction is simulated by MULTI-FS two-temperature Lagrangian 1D hydrodynamic model with multi-group radiation transport [2], improved. Next, for each Lagrangian cell, solution of hydrodynamic equations is post-processed by atomic kinetics code [3], which gives a distribution of ions over quantum states. Plasma density effects (continuum lowering, collectivization of bound states, etc.) are treated in the effective-statistical-weights approach]4]. In the atomic kinetics model, the cells interact due to radiation, which is determined as a multi-layer solution of the radiative transfer equation on a fine spectral grid. Spectral line shapes are affected by the Doppler broadening, cell-to-cell Doppler shifts caused by the plasma flow, and dynamic Stark effect. Besides the internal radiation field we simulate spectral intensity of radiation outgoing the spark in various directions. This allows to choose an optimal direction for installation of x-ray monochromator.

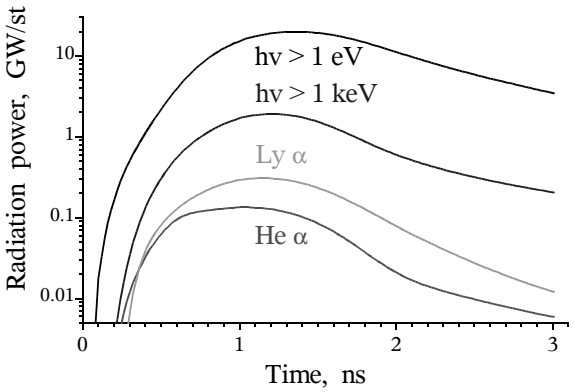

Fig. 1: The laser spark radiation power.

In the simulation shown in Figs.1 and 2, the laser pulse is focused on the 20-μm-thick aluminum foil. The laser wavelength is 1.06 μm, the pulse has a smooth $\sin^2(\pi t_{ns}/2_{ns})$ shape of 1 ns FWHM and peak intensity of 100 TW/cm^2 on the focal spot of 1 mm diameter. Fig.1 shows the laser spark radiation power emitted at 10° with respect to the spark axis. Peak x-ray power is 10% of the total radiation power; 16% of the x-rays belong to Lyman-α line. The x-ray power is high while the spark is fed by the laser. After the laser pulse, the radiation power goes down qickly, therefore a backlighter, driven by a sub-ns laser, provides temporal resolution of 1 ns with no shutter.

Fig. 2 shows the laser spark radiation yield at 10° with respect to the spark axis. The total yield is 28 J/sr. The x-ray yield is 8% of the total. The highest yield is observed in the 0.2 – 0.5 keV domain. One can see that spectral lines of Li-like ions are stronger than the x-ray lines. Lines emitted by lower (than Li-like) ionization stages are weak. Analysis shows that in inner plasma layers these lines are much stronger than at the outer plasma boundary; however, their intensity decreases significantly along the line of sight, mainly due to photo-ionization of excited ions.

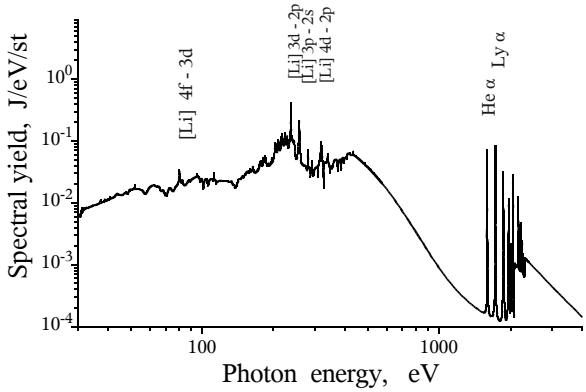

Fig. 2: The laser spark radiation yield.

The simulation showed that x-rays originate from narrow plasma layer where the density is not yet low while the temperature is already high. Thickness of this layer is 50 μm in the peak power. Laser light can penetrate into much denser plasma (therefore, heat much denser plasma) if the second harmonics of the laser is used. The increase in density is by a factor of 4 for electrons and even more for ions, because denser plasma is colder and less ionized. We predict that a laser spark generated by shorter-λ laser will be much brighter in x-rays, especially in the hard continuum. Note that small thickness of the x-ray-emitting layer together with the small distance between this layer and initial location of the foil justify the 1-D approach to the problem.

Alternatively to the laser spark, a 1-2 MA z-pinch may be used for x-ray backlighting the heavy-ion-beam targets. Table-top z-pinches of MA class are reliable, easy-to-use devices that give x-ray power on GW/sr level in pulses of 8-15 ns duration.

[1] The letter of intent for HEDgeHOB project, 2004.
[2] K. Eidmann et al., Phys. Rev. E 62, 1201 (2000).
[3] V. I. Fisher et al., unpublished.
[4] D. V. Fisher and Y. Maron. JQSRT 81, 147 (2003).

[1]Weizmann Institute of Science, Israel
[2]Soreq NRC, Israel;

Plasma heating with laser-driven hohlraum radiation

E. Baldina, T. Schlegel, J. Maruhn

Laser-driven hohlraums are excellent devices for spatially homogeneous heating of matter up to the plasma state. In laser-based IFE research for example, this indirect drive scheme allows to meet the high spatial symmetry demands for pellet compression. Soft x-ray hohlraum radiation was also applied successfully in material research, e.g shock wave propagation and opacity measurements. Related databases are of large importance for research in plasma physics as well as in studies of geo- and astrophysical problems.

A basic question in heavy ion matter interaction at high beam particle intensities is the energy deposition of fast ions in hot plasmas. At recent beam intensities, the hot plasma must be prepared by a seperate driver providing sufficiently smooth density and temperature profiles on the characteristic space and time scales of the ion plasma interaction.

The design of corresponding hohlraum targets is in general a 3D problem, taking into account discontinuities of initial and boundary conditions, angular anisotropy of absorbing and reflecting properties of the wall material or the asymmetric laser illumination. In addition, a multigroup kinetic approximation of radiation transport is necessary. The optimum numerical approach for modeling the radiation exchange between the hohlraum walls is the solution of the integral transport equation solved with the view factor method [1]. This model must be coupled to a 1D Lagrangian hydrocode including multigroup kinetic radiation transport [2].

Usually, the hohlraum will be splitted into many sectors, which can have different geometry, material composition, boundary conditions, external energy deposition, or they are heated only by incident hohlraum radiation. The distribution of the radiation temperature on the inner surface of the hohlraum walls, e.g. a hollow gold cylinder (radius 0.5 mm, length 0.5 mm) closed at both ends with gold foils, is given in Fig. 1. A laser beam with a Gaussian intensity profile and a $\sin^2$ pulse shape illuminates the external surface of one of the closing discs in this example. The pulse duration is 1 ns (FWHM), peak laser intensity amounts to 2×10^{13} W/cm^2 for a beam radius of 0.33 mm (FWHM). The full laser energy is approximately 40 J. At the end of the pulse, the hohlraum is heated up to radiation temperatures of more than 20 eV also at the initially cold ends of the cylinder (sectors 6 and 10). When the hohlraum is open on the side opposite to the laser incidence, the radiation temperature will be smaller due to losses through the open hole.

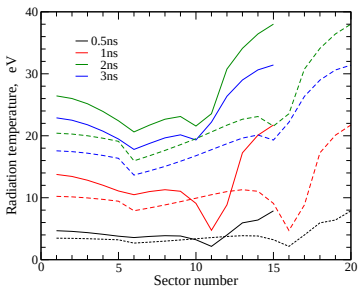

Figure 1: Closed cylindrical hohlraum with gold walls (left disc: sectors 1 - 5, cylindrical wall: sec. 5 - 10, laser-illuminated right closing foil: sec. 11 - 15). Dashed lines correspond to a two times longer hohlraum.

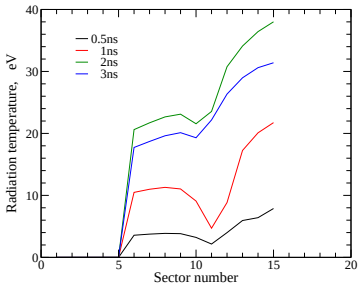

Figure 2: Same cylindrical hohlraum as in the previous figure but with open left side.

If the inner surface of an open cylindrical case is heated by the laser beam with similar pulse parameters and an overall energy of only 20 J, we get even higher temperatures, because most of the laser energy converted to x-rays is trapped in the hohlraum. Fig. 3 shows a rather homogeneous radiation energy distribution after the laser heating.

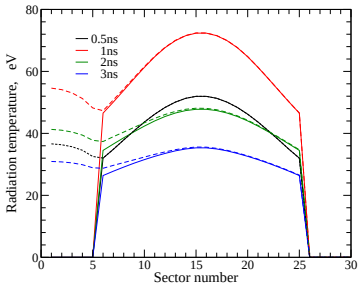

Figure 3: Internal heating of an open cylindrical hohlraum of 2 mm length with a 20 J laser pulse. Dashed lines show the results for a partly closed case.

Modeling with radiation transport in grey approximation inside the walls shows a strong deviation from the multigroup approach. Therefore, hohlraum design with help of the 2D MULTI code in its present state does not allow to get quantitatively correct results.

[1] E. G. Baldina, "Multigroup kinetic description of x-ray transport in hohlraums", Laser and Particle Beams, **22**, 65 (2004).
[2] K. Eidmann et al., "Hydrodynamic simulation of subpicosecond laser interaction with solid-density matter", Phys. Rev. E, **62**, 1202 (2000).

Higher harmonics from short-pulse laser irradiation of solid targets

U. Teubner, K. Eidmann, T. Schlegel, P. Gibbon

When short-pulse laser light with large values of $I\lambda_0^2 \approx 10^{18}(\mathrm{W/cm^2})\mu\mathrm{m}^2$ and higher, where I is the laser intensity and λ_0 the laser wavelength, hits a solid target surface, high harmonics will be generated. Besides intense high-order harmonics in the reflected light from the front side of a solid target, which can show interesting intensity modulations [1], harmonics up to the tenth order including the fundamental from the rear side were observed [2].

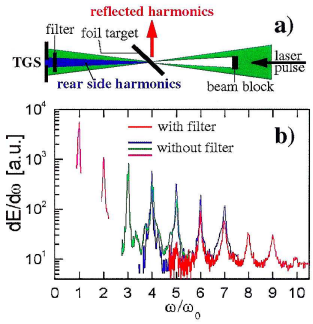

Figure 1: (a) Scheme of the experimental setup. (b) Typical harmonic spectra measured at the rear side of a 60nm carbon foil which was illuminated by 150 long frequency-doubled and p-polarized Ti:sapphire laser pulses at $\lambda = 395$ nm, peak intensities up to 5×10^{18} W/cm^2 and an angle of incidence 45^o.

Hydrodynamic calculations with the MULTI-FS code [3], using the temporal shape of the applied laser pulse including the residual weak prepulse as input, showed that the foils expand only slightly during the interaction with the laser pulse. Because in this almost one-dimensional expansion the areal mass is conserved, the target remains overdense for the laser and the harmonics from the rear side cannot be interpreted as transmitted light from the front surface.

Kinetic simulations with the one-dimensional LPIC code [4], which allows to model the experimental conditions - oblique incidence 45^o relative to the target normal at p polarization- reproduced the main features of the experiment. The sharp cutoff in the harmonic spectrum at plasma frequency, corresponding to the maximum electron density in the target, is demonstrated in Fig.2. With an initially lower target density, the cutoff changes to a corresponding lower value, although areal mass was kept constant.

The PIC simulations also show that bunches of energetic electrons are generated in the laser-irradiated front surface of the target and propagate periodically with the laser frequency through the foil to the rear side. Because the accelerating electric field of the laser-induced plasma wave is strongly anharmonic, the electron current contains higher harmonics of the laser frequency. Fig.4 shows the corresponding Fourier transform of the longitudinal electron current at different locations in the target. In the center of the foil, where $n_e/n_c \approx 80$, the frequency $9\omega_0$

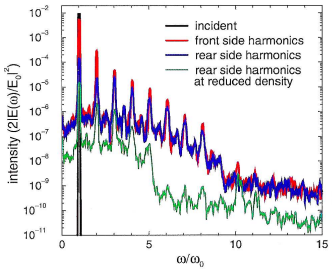

Figure 2: Simulated front (red) and rear side (blue) spectra ($n_e/n_c = 84$). The green line for the case of an initial density $n_e/n_c = 27$ is shifted down by a factor of ten for clarity.

clearly dominates in the j_x spectrum, corresponding to the local plasma frequency $\omega_p/\omega_0 = \sqrt{n_e/n_c} \approx 9$. In the same way, the 5th and 6th harmonics dominate at $n_e/n_c \approx 30$, where the corresponding resonances are excited, and the fundamental at $n_e/n_c \approx 1$, respectively. Due to obliquely incident laser light the electron current has also a transverse component j_y. Both j_x and j_y depend on the y coordinate by the same phase factor as the incident wave vector. Consequently, these currents are a source of electromagnetic radiation, which is emitted from the rear side with the same direction and polarization as the incident light.

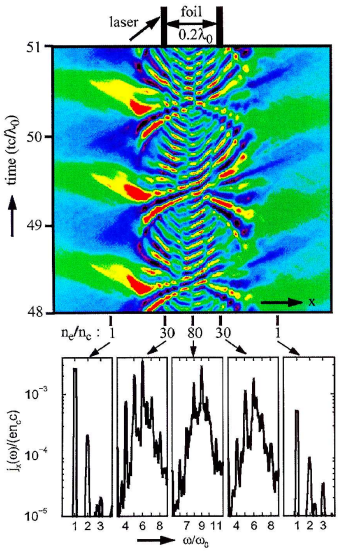

Figure 3: Current density j_x along the target normal. Red correponds to maximum positive, blue to maximum negative values, and green to zero.The thick bars indicate the unperturbed foil at $t = 0$.

[1] U. Teubner et al., Phys. Rev. A, **67**, 013816 (2003).
[2] U. Teubner et al., Phys. Rev. Lett., **92**, 185001 (2004).
[3] K. Eidmann et al., Phys. Rev. E, **62**, 1202 (2000).

3. First investigations on possible PHELIX – specific experiments

The first aim of the ILIAS study group is to propose and to elaborate concepts for the first ultrashort PHELIX laser beam. This is expected to deliver 10 Joules in 500 fs and focusable to yield the energy flux density of $I = 10^{19}$ W/cm². In addition, a good contrast ratio is compulsory, with a desirable prepulse intensity not exceeding 10^{13} W/cm².
Promising experiments with such a beam can be performed on

3D simulations on beam-target interaction
Determination of the effective critical density for laser energy deposition
Spectra of fast electrons and ions from overdense targets; origin of fast ions (front/tear side of the target)
Fast electron transport
Efficient Generation of high harmonics of the laser frequency
Shock generation for equation of state (EOS) investigations in dense matter
Laser-ion beam interaction (multiphoton effects, relativistic atomic physics)

There is strong international competition on most of these projects. ILIAS has a vivid interest in elaborating GSI-specific experiments which consist in using both, the PHELIX laser and the heavy ion beam in combined projects. In one of the following contributions a first attempt is made in this direction (P. Mulser/W. Scheid). Significant contribution to understanding the origin of fast ions is expected from the molecular dynamics-type tree-code in ILIAS which is one of the very few codes combining accurate collisional with free flow physics (P. Gibbon). Despite considerable expertise on electron acceleration by laser beams in ILIAS (W. Scheid) and the recent break-through in generating highly collimated nearly monoenergetic e-beams such studies must, perhaps, be postponed until a sub 10 fs beam option will be available in PHELIX.

Following:

P. Gibbon on

Proposed experiments on ion acceleration

P. Mulser, W. Scheid on

High-field atomic physics with PHELIX on relativistic heavy ion beams

Proposed experiments on ion acceleration

P. Gibbon

In the light of continuing controversy over proton acceleration mechanisms and new particle simulations using cold, collisional targets (see report by P. Gibbon), it would seem timely to carry out a series of investigative experiments to determine the relative characteristics and merits of proton beams generated at the front- and rear-side of solid foil targets. Modelling suggests that the front-side mechanism will dominant if the target can be kept cold before the main pulse strikes, which would require a *high contrast ratio* (e.g. 2^{nd} harmonic pump or plasma mirror scheme as recently demonstrated for harmonic generation from solid surfaces).

Some possible campaigns/avenues of investigation might be:

1. Use of H- or D-doped sandwich targets to improve the beam monochromaticity – e.g plastic layer at various distances from the front surface to delay onset of acceleration via ponderomotive force/hole-boring.

2. Is there a correlation/relation between electron absorption physics (see report by P. Mulser) and ion beam origin/characteristics? Experiments to date have tended to take for granted that relativistic 'jxB' heating dominates typical Petawatt interactions, which tend to have large prepulses/ preplasmas, yet this may not be the optimal configuration for ion acceleration – particularly from the front side. Earlier experience with PIC simulations has shown that obliquely incident light (on a steep gradient) might actually lead to stronger ion shocks (accompanied by faster blowoff) than for normal incidence. A further largely unexplored issue related to Fast Ignitor physics is the propagation and energy deposition of relativistic pulses in extended plasma profiles.

3. Use of ion beams to control/vary target conductivity in transport experiments. Many independent theoretical studies and experiments to date indicate a high sensitivity of hot electron penetration depth to the initial target state, which can be subjected to substantial preheating, ionization and even hydrodynamic expansion. Stricter control over target conditions might be achieved by using ion beams to preionize channels for hot electron flow, or to set up (3-dimensional) target regions with predefined resistivity prior to laser irradiation.

High-field atomic physics with PHELIX on relativistic heavy ion beams

P. Mulser and W. Scheid

When an atom or ion is exposed to intense laser radiation rapid ionization sets in. In the visible and near UV spectrum appreciable multiphoton ionization occurs starting at $I \approx 10^{12}$ W/cm². As long as the perturbing potential is by a factor of 5 smaller than the atomic potential the multiphoton process is well described by standard perturbation analysis of minimum order n if n is the number of photons to cover the energy gap between the bound and the free state. A typical measure of the ionization time is the inverse of the Rabi frequency $\omega_R = 2\pi\mu E/h$, μ dipole moment, E laser field. At 10^{12} W/cm² it is 50 times longer than the Nd laser period. With increasing laser energy above-threshold ionization (ATI), a level shift due to the dynamical Stark effect and higher level excitation become more and more important and higher order diagrams must also be considered. Latest from $I = 10^{16}$ W/cm² on the distortion of the Coulomb potential by the laser field can no longer be disregarded in the visible and near UV. This is the domain of optical field ionization. Its gross feature can be understood from a semiclassical model of "over the barrier" and tunnel ionization [1]. For gold (Au^{79}) 20 fold and 50 fold ionization at $I = 10^{18}$ and $I = 10^{20}$ W/cm², respectively, is predicted.
Single multiphoton or field ionization is well understood. In principle nonsequential ionization is also clarified [1]. The mechanism is the same as for high-order ATI and high-order harmonic generation. In the first step the electron is detached from the core through tunneling and over the barrier ionization. In the second step it propagates in the continuum like a quasi-free electron accelerated by the laser field. In the third step the electron interacts with the core when its trajectory comes close to it. At this point the electron may (i) become scattered (high ATI), (ii) knock out other bound electrons (nonsequential ionization), or (iii) recombine radiatively and emit an energetic photon. This is the so-called rescattering model.
In detail, there are still open questions:

- Why does, quantitatively, He behave differently from Ne, and Ne differently from Ar?
- Do level spacings lying close to an integer number of laser photons make the difference?
- When does ionization stabilization occur and what can we learn from it?

By the latter phenomenon ionization inhibition despite increasing laser intensity is addressed. The theory predicts that it occurs for $h\omega/2\pi > E_{bound}$ and at the same time the oscillation amplitude of the "active" electron must exceed the radius of the atomic (ionic) core.
We claim that these three questions can be studied with a still moderate PHELIX laser beam counterpropagating to the relativistic heavy ion beam in the GSI storage ring. Such a combination offers tunability of the laser wavelength for studying

- the effect of resonances and level shifts on ionization,
- multiphoton ionization in the UV frequency domain,
- the efficiency of hard UV photon generation via high harmonics.

Access to such kinds of experiments is made possible in all three cases by the Doppler frequency upshift in counterpropagating ion beams. In such a configuration the following relations between the physical quantities in the lab frame (undashed) and in the frame of the ion beam at rest (dashed symbols) hold:

$$\omega' = \gamma(1 + v/c)\omega, \quad \boldsymbol{E}', \boldsymbol{B}' = \gamma(1 + v/c)\boldsymbol{E}, \boldsymbol{B}, \quad I' = \gamma^2(1 + v/c)^2 I \qquad (1)$$

At $\gamma = 30$ the ion beam is exposed to Nd photons of 60 eV instead of 1 eV energy and the intensity of $I = 10^{19}$ W/cm² is upconverted to $I' = 3.6 \times 10^{22}$ W/cm². In view of such promising perspectives it is worthwhile to calculate pertinent cross sections and rates of events. In a recent paper [2] the efficiency of high harmonic generation is studied for laser intensities of $I = 10^{17}$ W/cm². Already at such moderate Nd laser intensities quencing of harmonic generation by a factor of 1000 is calculated in the lab frame owing to the electron orbit distortion by the magnetic field of the laser beam. In contrast, with the harder photons corresponding to $\gamma = 15$ quencing is only by a factor of 3.5. Upconversion of ω and I may also studies of nuclear γ reactions make feasible.

[1] D. Bauer, *Intense laser field-induced multiphoton processes in single and many electron systems,* Habilitationsschrift, TU Darmstadt, 2002.
[2] C. C. Chirilä, C. J. Joachain *et al*., *Interaction of superintense laser pulses with relativistic ions*, Phys. Rev. Lett. 93, 243603 (2004).

4. Summary and conclusion

The ILIAS study group at GSI was founded in January 2005 by seven members with the intention of forming a nucleus for theoretical investigations in the emerging field of superintense laser interaction with dense matter and particle beams. The activity will comprise fundamental as well as applied research geared to supporting the experimental projects within PHELIX, intensifying the flow of ideas within the existing research groups and, eventually, to stimulating new directions in the field.

As a **first** step towards this ambitious goal the ILIAS group has:

- arranged a weekly seminar, open to interested theoreticians, experimentalists and to guests from outside, hosted at GSI
- prepared the report presented herein, containing the scientific profiles of the current members and describing their recent studies and achievements in the field.

Detailed expertise is available in

Numerical simulation:
Tree code molecular dynamics; 1D3V electromagnetic PIC (P. Gibbon)
Multidimensional hydrodynamic codes: 2 + 3D adaptive grid multifluid lagrangian – eulerian CFDLIB (J. Maruhn, Anna Tauschwitz),
hydrodynamic multigroup radiation code MULTI; 1D PIC; SNOP opacity code (T. Schlegel), radiation transport by view factor method (J. Maruhn, T. Schlegel).

Atomic and nuclear physics:
Short pulse dynamics, electron dynamics in strong laser and Coulomb fields, pair production, excitation of nuclear states (W. Scheid).

Laser energy conversion and energy transport:
Absorption, fast electrons, fast ion generation, collisional physics (P. Gibbon, P. Mulser).

Nonlinear Optics:
Harmonics, X-ray radiation (T. Schlegel, P. Gibbon).

There is considerable expertise available in the group. What needs to be done is more effective focusing on fertile ideas relevant for PHELIX, the first steps of which have already been realized. First fruits of the ILIAS seminar discussions are two sketches of proposals for possible experiments with the first ultrashort laser beam which should be available by the end of the year (Sec.3 of this report).

One of the next steps of ILIAS has to consist in raising the interest of the Theoretical Division of GSI and in creating a common basis of knowledge and discussion with its members in order to benefit from the available know how. We greatly acknowledge the interest already shown by K. Langanke and J. Wambach.
Finally, central effort is to be spent to attract young students from the neighbouring universities for diploma, PhD theses and postdoc applicants in the field of superintense laser and ion beam interactions with dense matter.